PRC1 fine-tunes gene repression and activation to safeguard skin development and stem cell specification

PRC1 fine-tunes gene repression and activation to safeguard skin development and stem cell specification

Idan Cohen[1], Dejian Zhao[2], Carmit Bar[1], Victor J. Valdes[1,3], Katherine L. Dauber-Decker[1], Minh Binh Nguyen[1], Manabu Nakayama[4], Michael Rendl[1,5], Wendy A. Bickmore[6], Haruhiko Koseki[7], Deyou Zheng[8], and Elena Ezhkova[1,9,*]

[1] Black Family Stem Cell Institute, Department of Cell, Developmental, and Regenerative Biology; Icahn School of Medicine at Mount Sinai; 1 Gustave L. Levy Place, New York, NY 10029; USA
[2] Department of Genetics; Albert Einstein College of Medicine; 1300 Morris Park Avenue, Bronx, NY 10461; USA
[3] Current address: Department of Cell Biology and Development, Instituto de Fisiologia Celular; UNAM; Mexico City, 04510; Mexico
[4] Department of Technology Development; Kazusa DNA Research Institute; 2-6-7 Kazusa-Kamatari, Kisarazu, Chiba 292-0818; Japan
[5] Department of Dermatology, Icahn School of Medicine at Mount Sinai; 1 Gustave L. Levy Place, New York, NY 10029, USA
[6] MRC Human Genetics Unit; MRC Institute of Genetics and Molecular Medicine at University of Edinburgh; Crewe Road, Edinburgh, EH4 2XU; United Kingdom
[7] Laboratory for Developmental Genetics; RIKEN Center for Integrative Medical Sciences (IMS) and CREST, Japan Science and Technology Agency; 1-7-22 Suehiro-cho, Tsurumi-ku, Yokohama, Kanagawa 230-0045; Japan
[8] Departments of Genetics, Neurology, and Neuroscience; Albert Einstein College of Medicine; 1300 Morris Park Avenue, Bronx, NY 10461; USA
[9] Lead Contact

*To Whom Correspondence Should be Addressed
Icahn School of Medicine at Mount Sinai
One Gustave L Levy Place, Box 1020
New York, NY 10029
elena.ezhkova@mssm.edu
Tel# 212-241-7184
Fax# 646-537-9695

Summary

Polycomb repressive complexes (PRC) 1 and 2 are essential chromatin regulators of cell identity. PRC1, a dominant executer of Polycomb-mediated control, functions as multiple sub-complexes that possess catalytic-dependent H2AK119 mono-ubiquitination (H2AK119ub) and catalytic-independent activities. Here, we show that despite its well-established repressor functions, PRC1 binds to both silent and active genes. Through *in vivo* loss-of-function studies, we show that global PRC1 function is essential for skin development and stem cell (SC) specification, whereas PRC1 catalytic activity is dispensable. Further dissection demonstrated that both canonical and non-canonical PRC1 complexes bind to repressed genes, marked by H2AK119ub and PRC2-mediated H3K27me3. Interestingly, loss of canonical PRC1, PRC1 catalytic activity, or PRC2 leads to expansion of mechanosensitive Merkel cells in neonatal skin. Non-canonical PRC1 complexes, however, also bind to and promote expression of genes critical for skin development and SC formation. Together, our findings highlight PRC1's diverse roles in executing a precise developmental program.

Keywords

Polycomb complex, PRC1, skin, epidermis, hair follicle, stem cells, Merkel cell, epigenetics

Introduction

It is becoming increasingly clear that chromatin regulators are critical factors controlling stem cells (SCs), tissue development, and homeostasis. Importantly, alterations in the functions of chromatin regulators lead to human diseases, including cancer (Vogelstein et al., 2013). Polycomb is a major chromatin regulator that functions as two multi-subunit complexes, Polycomb repressive complex (PRC) 1 and PRC2. PRC2 consists of the EED, SUZ12, and EZH1/2 core subunits, and establishes tri-methylation on H3K27 (H3K27me3) (Cao et al., 2002; Margueron and Reinberg, 2011). Several mammalian PRC1 sub-complexes have been identified (Gao et al., 2012), and each of them contains an E3 ubiquitin ligase, RING1A or RING1B, which catalyses H2AK119ub (de Napoles et al., 2004; Gao et al., 2012; Wang et al., 2004). At target genes, PRC1 and PRC2 compact chromatin and repress genes (Simon and Kingston, 2009), although a few examples of PRC1 and PRC2 subunits binding to active genes have been reported (Kloet et al., 2016; Mousavi et al., 2012; van den Boom et al., 2016). Recent studies demonstrated that PRC1 promotes H2AK119ub-dependent recruitment of PRC2, suggesting a pivotal role for PRC1 in Polycomb-mediated gene control (Blackledge et al., 2014; Cooper et al., 2014).

Surprisingly, while numerous loss-of-function studies of PRC2 have been reported (Chiacchiera et al., 2016b; Ezhkova et al., 2011; Ezhkova et al., 2009; Juan et al., 2011; Mu et al., 2014), the functions of PRC1 in somatic tissue development and tissue-specific SC control are largely unknown. Additionally, the importance of PRC1's E3 ubiquitin ligase activity has recently been debated and its importance for tissue control is unclear (Endoh et al., 2012; Illingworth et al., 2015; Pengelly et al., 2015). Finally, there are at least six different mammalian PRC1 sub-complexes, as defined by the specific PCGF1-6 subunits that compose the core PRC1 complex together with RING1A or RING1B (PRC1.1-PRC1.6) (Gao et al., 2012). These can be further divided into canonical PRC1 (cPRC1) complexes that contain PCGF2 or BMI1 (PCGF4) and a CBX protein, that recognizes H3K27me3 to facilitate cPRC1 recruitment to chromatin (Simon and Kingston, 2009). Non-canonical PRC1 (ncPRC1) complexes lack CBX proteins and their recruitment to chromatin is not dependent on H3K27me3 (Blackledge et al., 2014; Cooper et al., 2014). ncPRC1 complexes contain RYBP or its homolog YAF2, one of PCGF1-6 proteins, and other subunits (ncPRC1.1-ncPRC1.6). These complexes were shown to differ in their accessory subunit composition, functional characteristics, and genomic localization *in vitro* with minimal overlap between them (Gao et al., 2012). Such distinct functional characteristics were further

demonstrated by showing that ncPRC1.3/1.5 complexes cooperate with the AUTS2 transcription factor to promote gene expression in neuronal cells (Gao et al., 2014). In line with this, recent loss-of-function studies of PCGFs in ESCs highlight different roles for the different PRC1 complexes (reviewed in (Bajusz et al., 2018)). These functional discrepancies are also evident from *in vivo* studies. Mice lacking a cPRC1 subunit, *Bmi1* (*Pcgf4*), exhibit posterior transformations, neurological defects, and progressive loss of hematopoietic SCs, in part due to misregulation of the *Ink4A/Arf* locus (Jacobs et al., 1999). Furthermore, loss of cPRC1 subunits, *Bmi1* and *Pcgf2*, leads to embryonic lethality (Akasaka et al., 2001). Mice lacking ncPRC1's *Pcgf6* subunit are viable and fertile but have anterior transformations of the axial skeleton, whereas loss of *Pcgf3/5* results in female-specific embryonic lethality (Almeida et al., 2017; Endoh et al., 2017). While these studies clearly suggest discrete roles for the different PRC1 complexes, their roles in somatic SCs and tissue development remain poorly studied.

Here, we used the developing skin epithelium as a model to dissect the roles of PRC1 in the control of a somatic/tissue-specific SC. During development, a monolayer of embryonic epidermal progenitors gives rise to the epidermis, which provides protective barrier functions, the hair follicles (HFs), which are important for thermo-protection, and the Merkel cells, which mediate mechanosensations (Blanpain and Fuchs, 2009; Perdigoto et al., 2016). By coupling *in vivo* chromatin and gene expression profiling with loss-of-function studies, we uncovered critical and diverse roles of PRC1 complexes in the control of skin epithelium development through regulation of both silent and active genes.

Results

Genome-wide analysis of PRC1 binding reveals enrichment at both active and repressed genes

We have previously generated mice in which the PRC2 subunit EED was ablated in embryonic epidermal progenitors (*Eed* cKO) (Dauber et al., 2016). PRC2 loss-of-function led to the loss of H3K27me3 in all skin epithelial lineages (Figure S1A). Intriguingly, immunofluorescence (IF) and Western blotting analyses did not reveal significant differences in PRC1-dependent H2AK119ub in *Eed* cKO skins (Figures S1A and S1B), indicating that PRC1 can mono-ubiquitylate H2AK119 in the absence of PRC2. To build on this observation, we next analyzed the genome-wide distribution of H3K27me3, H2AK119ub, and core PRC1 subunit RING1B, in epidermal progenitors. By performing fluorescence-activated cell sorting (FACS), we

purified epidermal progenitors from newborn (P0) *Keratin* (*Krt)14-RFP* and *Krt10-H2B-GFP* mice (Figures S1C-E) and subjected the isolated cells to a chromatin immunoprecipitation (ChIP) assay, followed by high-throughput sequencing (seq), using two biological duplicates for each ChIP-seq data. Interestingly, comparison of ChIP-seq peaks for RING1B revealed that 49% of RING1B target genes did not contain peaks for H2AK119ub or H3K27me3 (Figure 1A, Table S1).

Based on the interesting genome binding of RING1B, we next performed ChIP-seq analyses of H3K4me3, H3K27ac, and H3K4me1, which are histone marks associated with active promoters and enhancers, followed by clustering analysis with ChIP-seq data for RING1B, H2AK119ub, and H3K27me3. The analysis revealed four RING1B-bound peak clusters. In clusters 1 and 2, we observed strong and broad ChIP-seq signals for RING1B, H2AK119ub, and H3K27me3, low signals for H3K4me1 and H3K4me3, and no H3K27ac signal (Figure 1B). Overall, ChIP-seq signals for cluster 1 were more widespread than those for cluster 2 (Figure 1B). The RING1B peaks for both clusters were enriched at promoter regions (Figure 1C), and high-throughput sequencing of RNA (RNA-seq) revealed that nearby genes were repressed in control epidermal progenitors, with mean expression levels of FPKM < 1 (Figure 1D). In contrast, genomic regions of clusters 3 and 4 had narrow and lower signals of RING1B binding, and low levels of H2AK119ub and H3K27me3 (Figure 1B). Interestingly, they also had high levels of H3K4me3, H3K4me1, and H3K27ac, suggesting that in these regions, RING1B was bound to promoters or enhancers of transcriptionally active genes (Figures 1B and 1C). The main differences between clusters 3 and 4 were relatively higher levels of repressive H3K27me3 mark and lower levels of active marks in cluster 3 compared to 4 (Figure 1B). RNA-seq analysis showed that genes in clusters 3 and 4 were expressed at levels significantly higher than those in clusters 1 and 2, with the highest expression in cluster 4 (Figure 1D). ChIP-seq analysis of PRC1 subunits RYBP and BMI1, which are present in two main forms of PRC1 sub-complexes, revealed that the majority of RING1B-bound genes in each cluster were co-bound by at least one of these PRC1 proteins (Figures 1E, S1F, and Table S1), suggesting that RING1B binds to these repressed and active genes in the context of a PRC1 complex. Intriguingly, gene ontology (GO) analysis revealed that clusters 1 and 2 contained genes of non-skin lineages, and clusters 3 and 4 were enriched for transcriptional regulators, components of signaling pathways, and chromatin modifying proteins (Figure 1F, Table S1). Many of these genes were known critical regulators of epidermal development and epidermal progenitors (Figure S1G, Table S1).

PRC1 global, but not catalytic, activity is required for skin morphogenesis and the establishment of a functional HF-SC compartment

We next performed functional studies of PRC1 using conditional PRC1-null mice, in which the essential E3 catalytic core of all PRC1 complexes, RING1A and RING1B, is ablated in embryonic epidermal progenitors. We crossed *Ring1a*-null *Ring1b* floxed mice with *Krt14-Cre* mice, in which Cre recombinase is expressed under the keratin 14 promoter, which is active in embryonic epidermal progenitors starting at embryonic day (E) 12 (Dassule et al., 2000) (*Krt14-Cre*; *Ring1a*$^{-/-}$ *Ring1b*$^{flox/flox}$ = 2KO). Furthermore, as our ChIP-seq data revealed that the presence of PRC1/RING1B at active and repressed genes correlated with different levels of H2AK119ub (Figures 1B and 1D), we also aimed to discriminate between the catalytic-dependent and -independent roles of PRC1. To accomplish this, we generated conditional PRC1 catalytic-inactive mice (*K14-Cre*; *Ring1a*$^{-/-}$ *Ring1b*$^{I53A/flox}$ = I53A), in which the *Ring1b* gene carries an I53A point mutation that abrogates its E3-ligase activity and the associated establishment of H2AK119ub (Illingworth et al., 2015). IF and Western blotting studies confirmed the absence of RING1B in the postnatal day (P) 0 skin epithelium of 2KO, but not I53A mice, whereas H2AK119ub was absent from the skin epithelia of both mice (Figures S2A-S2C). Interestingly, H3K27me3 was slightly reduced in 2KO and I53A skin (Figure S2C), suggesting that PRC2 can establish H3K27me3 independently of PRC1, as has recently been described (Illingworth et al., 2015).

Analyses of P0 I53A and 2KO mice revealed striking differences. While both mice lacked milk spots, 2KO but not I53A mice had shiny skin and an open eyelid phenotype (Figure S2D). Hematoxylin and eosin (H & E) staining revealed that the epidermis of 2KO mice was thinner than that of control mice, whereas the epidermis of I53A mice was normal (Figures 2A, 2B, S2E, S3F, and S3G). IF analysis showed thinning of differentiated epidermal layers positive for KRT10 (Figure 2C) and loricrin (LOR) (Figure 2D) in 2KO, but not I53A epidermis. P0 2KO HFs were significantly shorter and had aberrant morphology compared to both control and I53A HFs (Figures 2A and 2E). IF analysis of AE15 (Figure S2F) and AE13 (Figure 2F), markers of differentiated layers of HFs, showed their absence in 2KO HFs, but not in control or I53A HFs.

In developing HFs, HF-SCs are specified and can be visualized by the expression of transcription factors NFATc1 and SOX9, which are critical regulators of HF-SC quiescence and maintenance, respectively (Horsley et al., 2008; Kadaja et al., 2014). Strikingly, IF analysis revealed that while NFATc1-positive (+) and

SOX9(+) cells were present in control and I53A HFs, they were practically absent in 2KO HFs (Figures 2G and 2H). To further test if 2KO HF-SCs are aberrantly formed, we analyzed the formation of sebaceous glands, HF appendages that are specified from SOX9(+) HF-SCs during development and are fully functional postnatally (Nowak et al., 2008). Since I53A and 2KO mice die shortly after birth, in order to analyze the complete development of HFs, we performed full-thickness grafts of 2KO, I53A, and control skins onto the backs of recipient *Nude* mice (Figure S2G). Fourteen days after engraftment (P14), 2KO HFs were short, and lacked hair shafts and sebaceous glands, in comparison to I53A and control HFs, which were fully developed (Figures S2H and S2I). To test whether HF-SC are specified in 2KO skin, we analyzed the potential of these mice to repair wounds, as in response to injury, HF-SCs are known to contribute to epidermal wound repair (Nowak et al., 2008). To analyze wound repair, we performed a split-thickness grafting assay, in which the dermis and HFs from a P0 mouse are enzymatically separated from the epidermis and grafted onto the back of a *Nude* recipient mouse (Nowak et al., 2008) (Figure 2I). Fourteen days after engraftment, control and I53A grafts re-epithelialized the epidermis and formed hairs, whereas in 2KO grafts, wounds were still apparent and no HF formation was observed (Figure 2J). Importantly, re-epithelialized 2KO epidermis was positive for H2AK119ub (Figure 2K), indicating that the *Nude* epidermis, rather than 2KO HF-SCs, repaired the wound. In contrast, re-epithelialized epidermis in I53A grafts lacked H2AK119ub, confirming that the new epidermis was established by I53A HF-SCs (Figure 2K). Together, these analyses show that the PRC1 complex, rather than its catalytic activity, is grossly required for epidermis and HF development, and the establishment of functional HF-SCs.

PRC1 global activity is required for skin epithelium development independently of *Ink4a/Arf* repression

We did not observe any changes in apoptosis in 2KO or I53A skins (Figures S3A and S3H). Interestingly, while the proliferation of epidermal progenitors in 2KO and I53A was indistinguishable from that of controls, the proliferation of I53A and 2KO HF cells was reduced (Figures S3B-S3E, S3I and S3J). PRC1 is known to repress the *Ink4a/Arf* locus (Bracken et al., 2007; Jacobs et al., 1999; Xie et al., 2014), which encodes a cell cycle inhibitor, INK4A, and a pro-apoptotic protein, ARF (Serrano et al., 1996). We confirmed that the *Ink4a/Arf* genes are targets of PRC1-mediated repression in control, but not 2KO skin epithelium by performing H2AK119ub ChIP, followed by qPCR (ChIP-qPCR) analysis of *Ink4a* and *Arf* (Figure S3K). Additionally, by performing reverse transcription followed by qPCR (RT-qPCR) analysis, we show that *Ink4A*

and *Arf* are upregulated in 2KO HF cells compared to I53A and control cells (Figure S3L). To test if the observed alterations in 2KO mice were due to activation of the *Ink4a/Arf* locus, we crossed 2KO with *Ink4a/Arf*-null mice (Serrano et al., 1996) to generate 3KO mice. Histological and IF analyses demonstrated that the epidermal and HF alterations observed in 2KO skins were still present in 3KOs (Figures S3M-S3T), indicating that the 2KO phenotype is largely independent of *Ink4a/Arf* upregulation.

PRC1 global and catalytic repressive functions fine-tune the expression of silenced and active genes

To gain insight into the molecular mechanisms underlying the observed phenotypic alterations, we performed RNA-seq on FACS-purified P0 control, I53A, and 2KO samples enriched for epidermal progenitors or HF cells (Jensen et al., 2010). We observed 1,141 vs. 682 upregulated genes in 2KO and I53A epidermal progenitors, respectively, and 990 vs. 479 upregulated genes in 2KO and I53A HF cells, respectively, compared to their corresponding controls (Figures 3A, S4A, and Tables S2, and S3). There was significant overlap in genes upregulated in I53A and 2KO cells; however, a large number of the genes upregulated in 2KO but not I53A was observed (Figures 3B and S4B). This suggests that both catalytic-dependent and -independent PRC1 activities provide critical layers of gene repression. Intriguingly, we also observed a large number of genes that were downregulated in 2KO, but not in I53A cells (Figures 3A, S4A, and Tables S2, and S3). We will return to these later.

By merging RNA-seq with ChIP-seq data, we observed that about 60% of upregulated genes were direct targets of RING1B and H2AK119ub (Figure 3C). ChIP analyses of I53A epidermal progenitors showed that RING1B remained globally bound to the genome (Figure S4C) and, importantly, to the genes that were upregulated in I53A cells (Figures S4D, S4J, and Table S2), whereas H2AK119ub was depleted at these genes (Figure S4E). This suggests that other global functions of PRC1 are maintained despite the loss of its catalytic activity. Genes upregulated in either I53A or 2KO cells were found in all four RING1B-bound clusters (Figure S4F) and the expression of these genes in control epidermal progenitors ranged from silenced/not expressed to lowly expressed (Figure S4G). Among the upregulated genes, we identified genes of non-skin lineages, as well as Merkel cell lineage genes (Figure 3D); these genes are normally repressed in epidermal progenitors (Table S1). We also identified epidermal genes that are lowly expressed in control epidermal progenitors (clusters 3 and 4) but are upregulated in 2KO or I53A cells (Figure 3D). Interestingly, some of

those genes are epidermal lineage genes known to promote either the proliferation or differentiation of epidermal cells. Collectively, these data show that PRC1 functions to repress unwanted lineage genes and attenuate the expression of epidermal lineage genes.

Loss of PRC1's catalytic activity recapitulates the PRC2-null Merkel cell phenotype

Further analysis of genes marked by H2AK119ub and upregulated in 2KO or I53A cells revealed that more than 70% of these genes were co-targeted by the PRC2-dependent H3K27me3 histone mark in control cells (Figure 3E). Remarkably, many of these upregulated genes were expressed in control cells (clusters 3 and 4) and had low, yet appreciated levels of H3K27me3 present around their transcriptional start sites (TSS) (Figure S4H). This indicates that PRC1 and PRC2 cooperate to repress silenced genes and attenuate the expression of active genes. Consistent with recent ESC studies (Illingworth et al., 2015), RING1B's catalytic activity and the lack of H2AK119ub affected PRC2's gene targeting, as we observed marked reductions in the global binding of PRC2's core subunit SUZ12 (Figure 3F) and H3K27me3 deposition (Figures S2C and S4I) in I53A epidermal progenitors compared to control cells. Importantly, the levels of SUZ12 and H3K27me3 were also drastically decreased at genes that were upregulated in I53A cells (Figures S4J-S4L). We next rationalized that if PRC1's catalytic activity is necessary to maintain intact PRC2 chromatin binding, then I53A mice should recapitulate the skin phenotypes observed in mice lacking PRC2 in epidermal progenitors. We recently reported that in *Suz12* conditional knockout mice (*Suz12* cKO), in which essential PRC2 subunit SUZ12 is ablated in embryonic epidermal progenitors, there is an increase in the number of Merkel cells (Dauber et al., 2016). Indeed, by performing IF analysis of Merkel cell markers KRT8 and SOX2 (Perdigoto et al., 2016), we observed a drastic increase in the number of Merkel cells in I53A skins compared to control skins (Figures 3G and 3H). Together, our data show that while the catalytic activity of PRC1 seems to be dispensable for the gross development of mouse skin, it is critical for maintaining proper PRC2 gene binding and repressing non-skin and Merkel cell lineage genes in epidermal progenitors.

Global and catalytic activities of PRC1 can repress genes independently of PRC2

As our data show that PRC1 catalytic activity maintains PRC2 binding, we next asked whether or not PRC1's gene repressive role is dependent on PRC2. We thus selected genes targeted by both PRC1 and

PRC2 and analyzed their expression in *Eed* cKO, I53A, and 2KO epidermal cells compared to controls. We observed two categories of genes. In the first category, we observed genes upregulated in both *Eed* cKO and 2KO epidermal cells (Figure 3I). Some of these genes were also upregulated in I53A cells (Figure 3I). We concluded that the genes of the first category require PRC1's global or catalytic activity, as well as PRC2 for their repression. In the second category, we identified genes that are upregulated in 2KO and/or I53A cells, but not in *Eed* cKO cells (Figure 3I), suggesting that the repression of these genes depends on PRC1 activity, but is maintained in the absence of PRC2. Probing deeper, we found that genes upregulated in both 2KO and I53A cells remained bound by RING1B the despite loss of H2AK119ub in I53A cells (Figures 3J- 3L, and S4J). Taken together, our data show that gene repression can be maintained through either PRC1/2-dependent or PRC1-dependent, PRC2-independent mechanisms. We also show that PRC1's catalytic activity alone can repress genes.

PRC1 binding positively regulates the expression of key skin developmental genes

We next revisited our RNA-seq data to analyze genes that were downregulated in 2KO and I53A cells. While 452 genes were downregulated in 2KO epidermal progenitors, only 73 genes were downregulated in I53A cells (Figures 3A, 4A and Table S2). GO analysis showed that among genes downregulated in 2KO populations were genes related to epithelium and epidermis development (Figure 4B and Table S2). By performing RT-qPCR analysis, we confirmed the RNA-seq finding and showed that while the expression of these genes was significantly reduced in 2KO cells, their expression was largely unaffected in I53A cells (Figure 4C). Importantly, among 2KO downregulated genes, our analysis revealed key epidermal signature genes and transcription factors, including *Satb1*, *Pou3f1*, *Ascl2*, *Ahr*, *Jun*, and *Grhl2* (Figure 4C), which were shown to have critical roles in epidermal development and function (Andersen et al., 1997; Chen et al., 2012; Fessing et al., 2011; Haas et al., 2016).

By matching our RNA-seq data with ChIP-seq data for RING1B, we observed that over 20% of downregulated genes were bound by RING1B. The majority of these downregulated genes with significant RING1B binding were in clusters 3 and 4 (Figure S5A), in which the levels of active histone marks were high and the level of PRC2-dependent H3K27me3 was low (Figure 1B). Comparing the levels of H3K27me3 in upregulated and downregulated genes in 2KO epidermal cells revealed that downregulated genes had

significantly lower levels of H3K27me3 compared to upregulated genes (Figure S5B). ChIP-qPCR analysis confirmed the ChIP-seq data and showed the presence of RING1B and H3K27ac (Figures 4D- 4F), as well as low levels of H3K27me3 and H2AK119ub at the promoter regions of these genes (Figures S5C and S5D). ChIP-qPCR for PRC1 subunits RYBP and BMI1 showed RYBP binding to these genes and BMI1 co-binding to a subset (Figures S5E and S5F), confirming that PRC1/RING1B works as a complex to promote gene expression in epidermal progenitors.

Analysis of HF cells also revealed that while 477 genes were downregulated in 2KO, only 71 genes were downregulated in I53A HF cells (Figures 4G, S4A and Table S3). GO analysis showed that among genes downregulated in 2KO populations were genes related to cell cycle, skin epithelium and HF development (Figure S5G and Table S3). By performing RT-qPCR analysis, we confirmed the RNA-seq data and showed that critical genes essential for HF development and homeostasis were downregulated in 2KO cells compared to control or I53A cells (Figure 4H). These included ORS genes, such as *Vdr*, *Lgr5*, and *Nfib*, HF matrix genes, including *Shh*, *Hoxc13*, and *Msx2*, and HF-SC genes, such as *Nfatc1* and *Lrig1* (Rezza et al., 2016). Concurrent with the observed decreased expression of *Shh* in 2KO HF matrix cells (Figure 4H), the expression of SHH signaling-responsive genes was also decreased in 2KO epidermal progenitors (Figure 4C). This was not due to changes in WNT signaling (Figures S5K and S5L), a known upstream regulator of SHH signaling in the developing skin. As recent studies showed that epidermal SHH signaling is required for Merkel cell specification (Perdigoto et al., 2016), we thus analyzed whether 2KO mice exhibit defective Merkel cell formation. Indeed, IF analysis of Merkel cell markers KRT8 and SOX2 showed a drastic reduction in the number of Merkel cells in 2KO compared to control skins (Figure S5M). The observed phenotype was not due to apoptosis (Figure S5N). Furthermore, we revealed a drastic reduction in the expression of *Atoh1* (Figure S5O), a critical early differentiation Merkel cell transcription factor. These data are intriguing, as they reinforce the observed gross phenotypic differences in mice with global epidermal loss of the PRC1 complex (2KO) versus mice with loss of its catalytic activity (I53A), in which an increase in the number of Merkel cells was observed (Figures 3G and 3H).

We next isolated HF-SC, ORS, and matrix cells as previously described (Wang et al., 2013) and subjected the purified cells to ChIP with antibodies against RING1B, H3K27ac, H3K27me3, and RYBP. Similar to our analysis of epidermal progenitors, ChIP-qPCR revealed the presence of RING1B around the

promoter/enhancer regions of critical HF-SC, ORS, and matrix genes (Figures 4I-4L), all of which we found to be downregulated in 2KO HFs (Figure 4H and Table S3). Additionally, H3K27me3 was absent (Figures S5H-S5J), whereas the H3K27ac histone mark was present at the promoters of these genes (Figures 4J-4L). RYBP was also present at the promoters of most genes (Figures S5H-S5J). Overall, we concluded that a PRC1/RING1B complex binds to and promotes the expression of critical epidermal and HF developmental genes.

To further test the direct role of PRC1 in promoting gene expression, we established *K14-CreER*; *Ring1a*$^{-/-}$ *Ring1b*$^{flox/flox}$ epidermal progenitor culture, in which *Ring1b* can be knocked out by 4-Hydroxytamoxifen (4-OHT) treatment. Treatment with 4-OHT led to a gradual reduction in the levels of RING1B protein and its corresponding H2AK119ub histone mark (Figure 5A). Concomitant with the decrease in RING1B global protein level, we observed a gradual reduction in RING1B binding to its target genes, which in turn correlated with changes in gene expression (Figures 5B and 5C). Indeed, we observed a gradual reduction in the expression of RING1B target genes that we found to be downregulated *in vivo* in 2KO epidermal cells (Figures 4C and 5C). Similar patterns were observed for genes repressed by PRC1, which became gradually upregulated (Figure S6A and S6B). To further establish the direct role of RING1B as a positive regulator, we overexpressed wild type and catalytic-inactive RING1B in wild type epidermal progenitors (Figure 5D) and observed an increase of RING1B binding to its target genes and an upregulation of target gene expression (Figures 5E and 5F). Taking these data together, we concluded that RING1B directly binds to and promotes the expression of many genes in epidermal progenitors independently of its catalytic activity.

cPRC1 and ncPRC1 complexes co-regulate skin development and skin stem cell specification

Interestingly, the different PRC1 complexes have been shown to differ in their genomic localizations *in vitro*, with only small overlap between different PCGF subunits (Gao et al., 2012). However, genome-wide targeting of these complexes in somatic SCs *in vivo* as well as their functional roles in tissue regulation and SC control is largely unknown.

To gain insight into the genomic localization of cPRC1 and ncPRC1 complexes in epidermal progenitors *in vivo*, we next performed ChIP-seq analyses of BMI1(PCGF4) (cPRC1.4 and ncPRC1.4), CBX8

(cPRC1.2 or cPRC1.4), RYBP (ncPRC1.1-PRC1.6), KDM2B (ncPRC1.1), and L3MBTL2 (ncPRC1.6). In particular, we investigated how these PRC1 components co-localized with RING1B by analyzing their ChIP-seq signals across the RING1B peak clusters described in Figure 1A. Our analysis revealed that BMI1 (PCGF4) and CBX8 were mainly present at RING1B-bound regions of clusters 1 and 2, whereas L3MBTL2 was present at RING1B-bound regions of clusters 3 and 4 (Figure 6A, 6B). RYBP and KDM2B, however, had more widespread binding across all four RING1B-bound clusters, but generally at a higher level in clusters 3 and 4 (Figures 6A, 6B). This difference became more apparent when the ChIP-seq signals of these PRC1 components were averaged over peaks in each of the four clusters, with the differences ranging from 2 to 6 fold (Figure S7A).

We analyzed which PRC1 complexes bind to genes that change their expression in 2KO cells. We thus selected genes that were upregulated in 2KO cells compared to control (2KO-up), suggesting a repressive role of PRC1 in the regulation of their expression. We also selected genes that were downregulated in 2KO epidermal progenitors (2KO-down), suggesting that PRC1 functions to promote the expression of these genes. By performing ChIP-qPCR in control epidermal progenitors, we detected binding of RYBP, a general subunit of all ncPRC1 complexes, to both gene classes (Figure 6C). Similarly, PCGF1 and KDM2B, subunits of ncPRC1.1 complex, were bound to both 2KO-up and 2KO-down genes (Figure 6D). Interestingly, BMI1(PCGF4) and CBX8, subunits of cPRC1.4 complex, were largely present at 2KO-up genes, whereas PCGF6 and L3MBTL2, subunits of the ncPRC1.6 complex, were present at 2KO-down genes (Figures 6E and 6F). These findings are consistent with our global analysis (Figure 6A). From these results, we concluded that cPRC1 complexes primarily target inactive, PRC1-repressed genes, while ncPRC1 complexes have more widespread binding and are present at both active and inactive genes. Importantly, genes downregulated in 2KO epidermal cells are co-targeted by different ncPRC1 complexes, suggesting a redundant role of these complexes in promoting their expression.

To explore the role of individual PRC1 complexes in the control of skin development and SC specification, we generated skin conditional *Pcgf1-6* knockout mice, in which an individual *Pcgf* gene is ablated in epidermal progenitors by crossing *Pcgf* flox/flox mice with *K14-Cre* mice. Due to reported functional redundancy between the close homologs *Pcgf2* and *Pcgf4*, as well as between *Pcgf3* and *Pcgf5* (Akasaka et al., 2001; Almeida et al., 2017), we also generated *Pcgf2/4* cKO and *Pcgf3/5* cKO mice. Western blotting

analysis of epidermal cells isolated from P0 *Pcgf1* cKO, *Pcgf2/4* cKO, *Pcgf3/5* cKO, and *Pcgf6* cKO mice confirmed the specific ablation of the PCGF protein targeted by Cre-mediated deletion (Figures S7B-E). Interestingly, loss of *Pcgf2/4* resulted in a decreased level of RING1B while no changes in H2AK119ub level were observed, while loss of *Pcgf3/5* resulted in decreased level of H2AK119ub mark (Figures S7C-S7G). We thus concluded that Pcgf3/5-containing ncPRC1 complexes are responsible for the deposition of the majority of H2AK119ub in the skin epithelium. Additionally, we observed only minimal overlap between RING1B binding and the accessory PCGF3/5 subunit AUTS2 (Table S4), suggesting that the majority of ncPRC1.3/5 in epidermal progenitors lack AUTS2.

Analysis of the epidermis of P0 *Pcgf1* cKO, *Pcgf2/4* cKO, *Pcgf3/5* cKO, and *Pcgf6* cKO mice compared to controls did not reveal any gross abnormalities, changes in thickness, or expression of epidermal differentiation markers KRT10 and LOR (Figures 6G, 6H, S7H and S7I). Similarly, no gross changes in HF formation or length were detected (Figures 6G and 6I). All knockout HFs expressed proper HF differentiation markers, AE13 and AE15, and contained SOX9(+) and NFATc1(+) cells, suggesting that the HF-SC compartment was appropriately specified (Figures 6J and S7J-L). This is different from the phenotype observed in 2KO mice, in which drastic changes in the formation of the epidermis and HFs were observed (Figures 2A-H). Notably, we observed an increase in the number of KRT8(+) Merkel cells in *Pcgf2/4* cKO skins (Figure 6K). Combining our biochemical and genetic analyses of different PRC1 complexes, we concluded that cPRC1 complexes function to repress the Merkel cell lineage, whereas different ncPRC1 complexes function redundantly to control the formation of the epidermis and HFs, and the specification of HF-SCs.

Discussion

Here we provide the first systematic analysis of PRC1 complexes in a mammalian SC system *in vivo*. Our data reveal diverse roles for Polycomb complexes in skin development and skin SC control. We show that in epidermal progenitors, PRC1 and PRC2 function together to silence non-epidermal and Merkel cell lineage genes, and to attenuate the expression of pro-proliferation and differentiation genes. Our data also reveal that PRC1 can function independently of PRC2 to promote the expression of genes that are critical for the development of the epidermis and HFs, and for the establishment of functional HF-SCs. Finally, we dissect the importance of cPRC1 and ncPRC1 complexes in the regulation of skin development, and highlight critical and

previously unappreciated roles for ncPRC1 complexes in tissue development. Together, our data reveal critical fine-tuning roles by which Polycomb complexes control the development of a mammalian tissue that is essential for our survival, the skin.

One of the hallmarks of PRC1 activity is the establishment of H2AK119ub (Simon and Kingston, 2009; Wang et al., 2004). Interestingly, the importance of PRC1's catalytic activity and the establishment of H2AK119ub for its repressive functions has been debated. In ESCs, RING1B is capable of repressing genes in the absence of its catalytic activity, whereas in *Ring1b*-null ESCs, there is a massive derepression of genes (Illingworth et al., 2015). Moreover, *in vivo* studies showed that RING1B's catalytic activity is dispensable for early embryonic development, whereas *Ring1b*-null mice die during gastrulation (Illingworth et al., 2015; Voncken et al., 2003). In line with findings in ESCs and mouse embryos, PRC1 repression of canonical Polycomb targets is maintained in catalytic-inactive PRC1-mutant *Drosophila* (Pengelly et al., 2015). In contrast to these studies, our work clearly shows that PRC1's catalytic activity is important for robust gene repression in epidermal progenitors. Importantly, in developing skin, loss of the catalytic activity of PRC1 leads to derepression of Merkel cell lineage differentiation genes and results in the formation of ectopic Merkel cells. We thus identified a precise functional role for PRC1's catalytic activity in a somatic tissue.

ESC studies recently showed that the catalytic activity of PRC1 is important for recruiting PRC2 to chromatin, and that loss of PRC1's catalytic activity leads to impaired deposition of H3K27me3 (Cooper et al., 2014; Illingworth et al., 2015). In I53A epidermal progenitors, the binding of PRC2 subunit SUZ12 and the levels of H3K27me3 were reduced, but still present at the chromatin. Consistent with these molecular findings, we observed similarities between the skin phenotypes that occur upon loss of PRC2 and upon loss of PRC1 catalytic activity. During embryogenesis, both PRC2-null and I53A mice exhibited normal gross epidermal and HF development, and showed similar ectopic Merkel cell formation.

However, despite the observed strong interplay and overlap between PRC1 and PRC2 in epidermal progenitors, our data clearly show that in the skin, the effects of complete loss of PRC1 (2KO mice) strikingly differ from those seen upon loss of PRC1 catalytic activity or the previously reported loss of PRC2 core subunits (Dauber et al., 2016; Ezhkova et al., 2011; Ezhkova et al., 2009). While the development of the epidermis and HFs was apparently intact in I53A and PRC2-null newborn mice, 2KO mice exhibited impaired skin epithelium development, and loss of Merkel cells and HF-SCs. Similar findings in phenotype severity were

recently reported in the adult mouse system, in which PRC1 functioned redundantly over PRC2 in the control of intestinal SC self-renewal (Chiacchiera et al., 2016a; Chiacchiera et al., 2016b). The observed phenotypic differences, however, are unlikely to stem only from the differential bindings of PRC1 and PRC2 complexes. Indeed, we showed that for a subset of genes that are co-bound by PRC1 and PRC2, loss of PRC1 led to derepression of these genes, while no marked changes in their expression were observed upon loss of PRC2. It is thus plausible to hypothesize that even upon co-targeting, PRC1 can sufficiently repress genes independently of PRC2, via catalytic-dependent and -independent mechanisms. Additionally, our findings also reinforce differences in the requirement for the global vs. catalytic activities of PRC1 for skin development.

The abundant literature on PRC1 is largely focused on the repressive roles of PRC1 in gene control. However, recent profiling of RING1B in ESCs and leukemic cells showed its binding to active genes (Kloet et al., 2016; van den Boom et al., 2016), but the functions of RING1B and PRC1 at these genes are yet unknown. Here, we show that in epidermal progenitors, PRC1 core subunit RING1B is present at transcriptionally active genes, where it can have either repressive or activating roles. At some active genes, PRC1 cooperates with PRC2 and attenuates gene expression, as loss of PRC1 leads to the upregulation of expression of these genes. We found that these genes typically have low, yet notable levels of H3K27me3 around their TSS. At other active genes, ncPRC1 binds in the absence of the H3K27me3 histone mark, and these genes typically have relatively lower levels of H2AK119ub. These genes include the master developmental regulator *Shh*, and critical SC regulators, such as *Nfatc1*, *Lgr5*, *Ascl2*, and *Jun*, which are also known to have important roles in other tissues, SCs, and/or cancers (Goodell et al., 2015; Hui et al., 2007; Singh et al., 2015). In these cases, PRC1 functions to promote the expression of these genes, as loss of PRC1 leads to downregulation of their expression, while overexpression of Ring1b *in vitro* leads to increased RING1B binding around the TSS and upregulation of the same epidermal genes. Our studies thus show diverse roles of PRC1 in regulating the expression of active genes.

By performing biochemical and genetic studies, we defined the roles of cPRC1 and ncPRC1 complexes in the control of skin development and SCs. We show that subunits of cPRC1 complexes largely target repressed genes that also contain H2AK119ub and PRC2-dependent H3K27me3 histone marks. The analysis of mice lacking *Pcgf2/4*, essential cPRC1 subunits, in embryonic epidermal progenitors revealed an increase in the number of Merkel cells, a phenotype that is also observed in PRC1-catalytically inactive mutant skins and

PRC2-null skins. Our data thus show that cPRC1 and PRC2 function together to repress the Merkel cell lineage differentiation program in epidermal progenitors.

Our profiling of genes targeted by subunits of ncPRC1 complexes revealed that they are present at both repressed and active genes. Moreover, we observed co-targeting of subunits of different ncPRC1 complexes to the same genes. This is in contrast to reported *in vitro* studies, in which each PRC1 complex preferentially targets a discrete subset of genes (Gao et al., 2012). Our analysis of skin epithelium-conditional knockout mice, in which individual ncPRC1 complexes are ablated in epidermal progenitors, showed that none of these mutant mice could recapitulate the *Ring1a/b* 2KO phenotype, where drastic alterations in the formation of the epidermis and hair follicles, and in the specification of HF-SCs were observed. Nonetheless, the fact that proper skin development was maintained in the absence of cPRC1 complexes (*Pcgf2/4* cKO) highlights the essential and previously unappreciated roles of ncPRC1 complexes in SC control and tissue development. Combining these genetic and biochemical data, we propose that ncPRC1 complexes have redundant functions in the regulation of skin development and skin SCs.

Collectively, our studies show that PRC1 plays a critical role in skin epithelium development. It does so by fine-tuning the expression of both active and repressed genes, and thus regulates the balance between cell proliferation and differentiation. RING1B and H2AK119ub are abundant in the human epidermis and are localized similarly to what is seen in murine epidermis (Figure S7M). Alterations in the expression and/or function of Polycomb subunits have been identified in many human maladies, including cancers (Koppens and van Lohuizen, 2016; Sauvageau and Sauvageau, 2010). Our identified roles for Polycomb provide future avenues for investigating the ways in which the misregulation of Polycomb functions, through gene repression and/or activation mechanisms, can lead to tumorigenesis.

Acknowledgments

For help, advice, and critical suggestions, we thank Xin Huang, Ramon Birnbaum, Anne Schaefer, Jianlong Wang, Ya-Chieh Hsu, Sergei Ezhkov, Venu Pothula, and Jose Silva. We are grateful for the assistance and reagents provided by Julie Segre and Elaine Fuchs. We thank Weipeng Mu and Terry Magnuson for the *Eed*$^{flox/flox}$ and *Suz12*$^{flox/flox}$ mice. We thank Philippe Soriano for the *Ink4a/Arf*$^{-/-}$ mice. We thank Rob Klose for his generous gift of the PCGF1 antibody. We thank Vivian Bardwell for her generous gift of the PCGF1 antibody. We thank the personnel of the Flow Cytometry Core Facility at the Icahn School of Medicine at Mount Sinai. V.J.V. was a Pew Latin American Fellow, supported by The Pew Charitable Trusts. C.B. is a Merksammer fund

scholar. K.L.D-D. was a trainee of the NIDCR-Interdisciplinary Training Program T32HD075735. W.A.B. is supported by a University Unit Programme Grant U127527202 from the UK Medical Research Council. The work of D.Y.Z. was supported by NIH/NHBLI grant R01 HL133120. Research reported in this publication was supported by the NIH/NIAMS under award numbers R01 AR063724 and R01 AR069078, and by the Tisch Cancer Institute under P30 Cancer Support Grant (E.E.). The content is solely the responsibility of the authors and does not necessarily represent the official views of the National Institutes of Health.

Author Contributions

I.C. and E.E. conceived and designed the experiments. I.C., V.J.V., C.B., K.L.D.D., and M.B.N performed the experiments. D.J.Z. and D.Y.Z. performed the bioinformatic analyses. M.R. provided *K14-RFP* and *Sox9-GFP* mice. H.K. provided the *Ring1a*$^{-/-}$, *Ring1b*$^{flox/flox}$ mice. M.N. and H.K. generated and provided *Pcgf1-6*$^{flox/flox}$ mice. W.A.B. provided the *Ring1b*^{I53A} mice. I.C., D.J.Z., D.Y.Z., and E.E. analyzed the data. I.C. and E.E. wrote the manuscript with input from all other authors.

Declaration of Interests

The authors declare no competing interests.

References

Akasaka, T., van Lohuizen, M., van der Lugt, N., Mizutani-Koseki, Y., Kanno, M., Taniguchi, M., Vidal, M., Alkema, M., Berns, A., and Koseki, H. (2001). Mice doubly deficient for the Polycomb Group genes Mel18 and Bmi1 reveal synergy and requirement for maintenance but not initiation of Hox gene expression. Development *128*, 1587-1597.

Almeida, M., Pintacuda, G., Masui, O., Koseki, Y., Gdula, M., Cerase, A., Brown, D., Mould, A., Innocent, C., Nakayama, M.*, et al.* (2017). PCGF3/5-PRC1 initiates Polycomb recruitment in X chromosome inactivation. Science *356*, 1081-1084.

Andersen, B., Weinberg, W.C., Rennekampff, O., McEvilly, R.J., Bermingham, J.R., Jr., Hooshmand, F., Vasilyev, V., Hansbrough, J.F., Pittelkow, M.R., Yuspa, S.H.*, et al.* (1997). Functions of the POU domain genes Skn-1a/i and Tst-1/Oct-6/SCIP in epidermal differentiation. Genes Dev *11*, 1873-1884.

Bajusz, I., Kovács, G., and Pirity, M.K. (2018). From Flies to Mice: The Emerging Role of Non-Canonical PRC1 Members in Mammalian Development. Epigenomes *2*, 4.

Blackledge, N.P., Farcas, A.M., Kondo, T., King, H.W., McGouran, J.F., Hanssen, L.L., Ito, S., Cooper, S., Kondo, K., Koseki, Y.*, et al.* (2014). Variant PRC1 complex-dependent H2A ubiquitylation drives PRC2 recruitment and polycomb domain formation. Cell *157*, 1445-1459.

Blanpain, C., and Fuchs, E. (2009). Epidermal homeostasis: a balancing act of stem cells in the skin. Nat Rev Mol Cell Biol *10*, 207-217.

Bracken, A.P., Kleine-Kohlbrecher, D., Dietrich, N., Pasini, D., Gargiulo, G., Beekman, C., Theilgaard-Monch, K., Minucci, S., Porse, B.T., Marine, J.C.*, et al.* (2007). The Polycomb group proteins bind throughout the INK4A-ARF locus and are disassociated in senescent cells. Genes Dev *21*, 525-530.

Cales, C., Roman-Trufero, M., Pavon, L., Serrano, I., Melgar, T., Endoh, M., Perez, C., Koseki, H., and Vidal, M. (2008). Inactivation of the polycomb group protein Ring1B unveils an antiproliferative role in hematopoietic cell expansion and cooperation with tumorigenesis associated with Ink4a deletion. Mol Cell Biol *28*, 1018-1028.

Cao, R., Wang, L., Wang, H., Xia, L., Erdjument-Bromage, H., Tempst, P., Jones, R.S., and Zhang, Y. (2002). Role of histone H3 lysine 27 methylation in Polycomb-group silencing. Science *298*, 1039-1043.

Chen, W., Xiao Liu, Z., Oh, J.E., Shin, K.H., Kim, R.H., Jiang, M., Park, N.H., and Kang, M.K. (2012). Grainyhead-like 2 (GRHL2) inhibits keratinocyte differentiation through epigenetic mechanism. Cell Death Dis *3*, e450.

Chiacchiera, F., Rossi, A., Jammula, S., Piunti, A., Scelfo, A., Ordonez-Moran, P., Huelsken, J., Koseki, H., and Pasini, D. (2016a). Polycomb Complex PRC1 Preserves Intestinal Stem Cell Identity by Sustaining Wnt/beta-Catenin Transcriptional Activity. Cell Stem Cell *18*, 91-103.

Chiacchiera, F., Rossi, A., Jammula, S., Zanotti, M., and Pasini, D. (2016b). PRC2 preserves intestinal progenitors and restricts secretory lineage commitment. EMBO J *35*, 2301-2314.

Cooper, S., Dienstbier, M., Hassan, R., Schermelleh, L., Sharif, J., Blackledge, N.P., De Marco, V., Elderkin, S., Koseki, H., Klose, R.*, et al.* (2014). Targeting polycomb to pericentric heterochromatin in embryonic stem cells reveals a role for H2AK119u1 in PRC2 recruitment. Cell Rep *7*, 1456-1470.

Dassule, H.R., Lewis, P., Bei, M., Maas, R., and McMahon, A.P. (2000). Sonic hedgehog regulates growth and morphogenesis of the tooth. Development *127*, 4775-4785.

Dauber, K.L., Perdigoto, C.N., Valdes, V.J., Santoriello, F.J., Cohen, I., and Ezhkova, E. (2016). Dissecting the Roles of Polycomb Repressive Complex 2 Subunits in the Control of Skin Development. J Invest Dermatol *136*, 1647-1655.

de Napoles, M., Mermoud, J.E., Wakao, R., Tang, Y.A., Endoh, M., Appanah, R., Nesterova, T.B., Silva, J., Otte, A.P., Vidal, M.*, et al.* (2004). Polycomb group proteins Ring1A/B link ubiquitylation of histone H2A to heritable gene silencing and X inactivation. Dev Cell *7*, 663-676.

del Mar Lorente, M., Marcos-Gutierrez, C., Perez, C., Schoorlemmer, J., Ramirez, A., Magin, T., and Vidal, M. (2000). Loss- and gain-of-function mutations show a polycomb group function for Ring1A in mice. Development *127*, 5093-5100.

Endoh, M., Endo, T.A., Endoh, T., Isono, K., Sharif, J., Ohara, O., Toyoda, T., Ito, T., Eskeland, R., Bickmore, W.A.*, et al.* (2012). Histone H2A mono-ubiquitination is a crucial step to mediate PRC1-dependent repression of developmental genes to maintain ES cell identity. PLoS Genet *8*, e1002774.

Endoh, M., Endo, T.A., Shinga, J., Hayashi, K., Farcas, A., Ma, K.W., Ito, S., Sharif, J., Endoh, T., Onaga, N.*, et al.* (2017). PCGF6-PRC1 suppresses premature differentiation of mouse embryonic stem cells by regulating germ cell-related genes. Elife *6*.

Ezhkova, E., Lien, W.H., Stokes, N., Pasolli, H.A., Silva, J.M., and Fuchs, E. (2011). EZH1 and EZH2 cogovern histone H3K27 trimethylation and are essential for hair follicle homeostasis and wound repair. Genes Dev *25*, 485-498.

Ezhkova, E., Pasolli, H.A., Parker, J.S., Stokes, N., Su, I.H., Hannon, G., Tarakhovsky, A., and Fuchs, E. (2009). Ezh2 orchestrates gene expression for the stepwise differentiation of tissue-specific stem cells. Cell *136*, 1122-1135.

Fessing, M.Y., Mardaryev, A.N., Gdula, M.R., Sharov, A.A., Sharova, T.Y., Rapisarda, V., Gordon, K.B., Smorodchenko, A.D., Poterlowicz, K., Ferone, G.*, et al.* (2011). p63 regulates Satb1 to control tissue-specific chromatin remodeling during development of the epidermis. J Cell Biol *194*, 825-839.

Gao, Z., Lee, P., Stafford, J.M., von Schimmelmann, M., Schaefer, A., and Reinberg, D. (2014). An AUTS2-Polycomb complex activates gene expression in the CNS. Nature *516*, 349-354.

Gao, Z., Zhang, J., Bonasio, R., Strino, F., Sawai, A., Parisi, F., Kluger, Y., and Reinberg, D. (2012). PCGF homologs, CBX proteins, and RYBP define functionally distinct PRC1 family complexes. Mol Cell *45*, 344-356.

Goldberg, A.D., Banaszynski, L.A., Noh, K.-M., Lewis, P.W., Elsaesser, S.J., Stadler, S., Dewell, S., Law, M., Guo, X., Li, X.*, et al.* (2010). Distinct Factors Control Histone Variant H3.3 Localization at Specific Genomic Regions. Cell *140*, 678-691.

Gong, S., Zheng, C., Doughty, M.L., Losos, K., Didkovsky, N., Schambra, U.B., Nowak, N.J., Joyner, A., Leblanc, G., Hatten, M.E.*, et al.* (2003). A gene expression atlas of the central nervous system based on bacterial artificial chromosomes. Nature *425*, 917-925.

Goodell, M.A., Nguyen, H., and Shroyer, N. (2015). Somatic stem cell heterogeneity: diversity in the blood, skin and intestinal stem cell compartments. Nat Rev Mol Cell Biol *16*, 299-309.

Haas, K., Weighardt, H., Deenen, R., Kohrer, K., Clausen, B., Zahner, S., Boukamp, P., Bloch, W., Krutmann, J., and Esser, C. (2016). Aryl Hydrocarbon Receptor in Keratinocytes Is Essential for Murine Skin Barrier Integrity. J Invest Dermatol *136*, 2260-2269.

Horsley, V., Aliprantis, A.O., Polak, L., Glimcher, L.H., and Fuchs, E. (2008). NFATc1 balances quiescence and proliferation of skin stem cells. Cell *132*, 299-310.

Huang da, W., Sherman, B.T., and Lempicki, R.A. (2009). Systematic and integrative analysis of large gene lists using DAVID bioinformatics resources. Nat Protoc *4*, 44-57.

Hui, L., Bakiri, L., Mairhorfer, A., Schweifer, N., Haslinger, C., Kenner, L., Komnenovic, V., Scheuch, H., Beug, H., and Wagner, E.F. (2007). p38alpha suppresses normal and cancer cell proliferation by antagonizing the JNK-c-Jun pathway. Nat Genet *39*, 741-749.

Illingworth, R.S., Moffat, M., Mann, A.R., Read, D., Hunter, C.J., Pradeepa, M.M., Adams, I.R., and Bickmore, W.A. (2015). The E3 ubiquitin ligase activity of RING1B is not essential for early mouse development. Genes Dev *29*, 1897-1902.

Jacobs, J.J., Kieboom, K., Marino, S., DePinho, R.A., and van Lohuizen, M. (1999). The oncogene and Polycomb-group gene bmi-1 regulates cell proliferation and senescence through the ink4a locus. Nature *397*, 164-168.

Jensen, K.B., Driskell, R.R., and Watt, F.M. (2010). Assaying proliferation and differentiation capacity of stem cells using disaggregated adult mouse epidermis. Nat Protoc *5*, 898-911.

Juan, A.H., Derfoul, A., Feng, X., Ryall, J.G., Dell'Orso, S., Pasut, A., Zare, H., Simone, J.M., Rudnicki, M.A., and Sartorelli, V. (2011). Polycomb EZH2 controls self-renewal and safeguards the transcriptional identity of skeletal muscle stem cells. Genes Dev *25*, 789-794.

Kadaja, M., Keyes, B.E., Lin, M., Pasolli, H.A., Genander, M., Polak, L., Stokes, N., Zheng, D., and Fuchs, E. (2014). SOX9: a stem cell transcriptional regulator of secreted niche signaling factors. Genes Dev *28*, 328-341.

Kloet, S.L., Makowski, M.M., Baymaz, H.I., van Voorthuijsen, L., Karemaker, I.D., Santanach, A., Jansen, P.W., Di Croce, L., and Vermeulen, M. (2016). The dynamic interactome and genomic targets of Polycomb complexes during stem-cell differentiation. Nat Struct Mol Biol *23*, 682-690.

Koppens, M., and van Lohuizen, M. (2016). Context-dependent actions of Polycomb repressors in cancer. Oncogene *35*, 1341-1352.

Li, H., Handsaker, B., Wysoker, A., Fennell, T., Ruan, J., Homer, N., Marth, G., Abecasis, G., Durbin, R., and Genome Project Data Processing, S. (2009). The Sequence Alignment/Map format and SAMtools. Bioinformatics *25*, 2078-2079.

Lien, W.H., Guo, X., Polak, L., Lawton, L.N., Young, R.A., Zheng, D., and Fuchs, E. (2011). Genome-wide maps of histone modifications unwind in vivo chromatin states of the hair follicle lineage. Cell Stem Cell *9*, 219-232.

Love, M.I., Huber, W., and Anders, S. (2014). Moderated estimation of fold change and dispersion for RNA-seq data with DESeq2. Genome Biol *15*, 550.

Margueron, R., and Reinberg, D. (2011). The Polycomb complex PRC2 and its mark in life. Nature *469*, 343-349.

Mousavi, K., Zare, H., Wang, A.H., and Sartorelli, V. (2012). Polycomb protein Ezh1 promotes RNA polymerase II elongation. Mol Cell *45*, 255-262.

Mu, W., Starmer, J., Fedoriw, A.M., Yee, D., and Magnuson, T. (2014). Repression of the soma-specific transcriptome by Polycomb-repressive complex 2 promotes male germ cell development. Genes Dev *28*, 2056-2069.

Nowak, J.A., Polak, L., Pasolli, H.A., and Fuchs, E. (2008). Hair follicle stem cells are specified and function in early skin morphogenesis. Cell Stem Cell *3*, 33-43.

Pengelly, A.R., Kalb, R., Finkl, K., and Muller, J. (2015). Transcriptional repression by PRC1 in the absence of H2A monoubiquitylation. Genes Dev *29*, 1487-1492.

Perdigoto, C.N., Dauber, K.L., Bar, C., Tsai, P.C., Valdes, V.J., Cohen, I., Santoriello, F.J., Zhao, D., Zheng, D., Hsu, Y.C.*, et al.* (2016). Polycomb-Mediated Repression and Sonic Hedgehog Signaling Interact to Regulate Merkel Cell Specification during Skin Development. PLoS Genet *12*, e1006151.

Rezza, A., Wang, Z., Sennett, R., Qiao, W., Wang, D., Heitman, N., Mok, K.W., Clavel, C., Yi, R., Zandstra, P.*, et al.* (2016). Signaling Networks among Stem Cell Precursors, Transit-Amplifying Progenitors, and their Niche in Developing Hair Follicles. Cell Rep *14*, 3001-3018.

Sauvageau, M., and Sauvageau, G. (2010). Polycomb group proteins: multi-faceted regulators of somatic stem cells and cancer. Cell Stem Cell *7*, 299-313.

Serrano, M., Lee, H., Chin, L., Cordon-Cardo, C., Beach, D., and DePinho, R.A. (1996). Role of the INK4a locus in tumor suppression and cell mortality. Cell *85*, 27-37.

Simon, J.A., and Kingston, R.E. (2009). Mechanisms of polycomb gene silencing: knowns and unknowns. Nat Rev Mol Cell Biol *10*, 697-708.

Singh, S.K., Chen, N.M., Hessmann, E., Siveke, J., Lahmann, M., Singh, G., Voelker, N., Vogt, S., Esposito, I., Schmidt, A.*, et al.* (2015). Antithetical NFATc1-Sox2 and p53-miR200 signaling networks govern pancreatic cancer cell plasticity. EMBO J *34*, 517-530.

van den Boom, V., Maat, H., Geugien, M., Rodriguez Lopez, A., Sotoca, A.M., Jaques, J., Brouwers-Vos, A.Z., Fusetti, F., Groen, R.W., Yuan, H.*, et al.* (2016). Non-canonical PRC1.1 Targets Active Genes Independent of H3K27me3 and Is Essential for Leukemogenesis. Cell Rep *14*, 332-346.

Vogelstein, B., Papadopoulos, N., Velculescu, V.E., Zhou, S., Diaz, L.A., Jr., and Kinzler, K.W. (2013). Cancer genome landscapes. Science *339*, 1546-1558.

Voncken, J.W., Roelen, B.A., Roefs, M., de Vries, S., Verhoeven, E., Marino, S., Deschamps, J., and van Lohuizen, M. (2003). Rnf2 (Ring1b) deficiency causes gastrulation arrest and cell cycle inhibition. Proc Natl Acad Sci U S A *100*, 2468-2473.

Wang, D., Zhang, Z., O'Loughlin, E., Wang, L., Fan, X., Lai, E.C., and Yi, R. (2013). MicroRNA-205 controls neonatal expansion of skin stem cells by modulating the PI(3)K pathway. Nat Cell Biol *15*, 1153-1163.

Wang, H., Wang, L., Erdjument-Bromage, H., Vidal, M., Tempst, P., Jones, R.S., and Zhang, Y. (2004). Role of histone H2A ubiquitination in Polycomb silencing. Nature *431*, 873-878.

Xie, H., Xu, J., Hsu, J.H., Nguyen, M., Fujiwara, Y., Peng, C., and Orkin, S.H. (2014). Polycomb repressive complex 2 regulates normal hematopoietic stem cell function in a developmental-stage-specific manner. Cell Stem Cell *14*, 68-80.

Ye, T., Krebs, A.R., Choukrallah, M.A., Keime, C., Plewniak, F., Davidson, I., and Tora, L. (2011). seqMINER: an integrated ChIP-seq data interpretation platform. Nucleic Acids Res *39*, e35.

Zhang, L., Stokes, N., Polak, L., and Fuchs, E. (2011). Specific microRNAs are preferentially expressed by skin stem cells to balance self-renewal and early lineage commitment. Cell Stem Cell *8*, 294-308.

Figure legends

Figure 1. Genome-wide analysis of PRC1 binding reveals enrichment at both active and repressed genes. (A) Overlap between RING1B, H2AK119ub, and H3K27me3 ChIP-Seq peaks in epidermal progenitors. (**B)** k-means clustering of ChIP-seq read densities across RING1B-peaks only, for duplicates of RING1B, and indicated histone modifications, with input signal subtracted. **(C)** Genomic distribution of RING1B peaks **(D)** Expression analysis of genes located near RING1B peaks in control epidermal progenitors. n=3. ***p<0.001; NS, not significant (one-way ANOVA with a Bonferroni post-hoc test). **(E)** IGV browser views of RING1B, H2AK119ub, H3K27me3, H3K27ac, RYBP, BMI1, and input for indicated representative genes for each RING1B-bound cluster. **(F)** Gene ontology (GO) analysis for RING1B target genes.
See also Figure S1 and Table S1.

Figure 2. Loss of PRC1 global, but not catalytic, activity leads to aberrant development of the epidermis and hair follicles (HFs), and failure to establish the HF stem cell (HF-SC) compartment. (A) Hematoxylin and eosin (H&E) analysis of P0 skins of *Krt14-Cre*; *Ring1a*$^{-/-}$ *Ring1b*$^{I53A/flox}$ (I53A; PRC1 catalytic-inactive mutant), *Krt14-Cre*; *Ring1a*$^{-/-}$ *Ring1b*$^{flox/flox}$ (2KO; PRC1-null), and control mice. Scale=100μm. (**B)**

Quantification of epidermal thickness. n=3. (**C-D)** IF staining for epidermal differentiation markers KRT10 (C) and LOR (D). **(E)** Quantification of HF length. n=3. **(F)** IF staining for AE13. (**G-H)** IF staining for HF-SC markers NFATc1 (G) and SOX9 (H). **(I)** Schematic representation of split-thickness engraftment. **(J)** Gross appearance of grafted skins 14 days post-grafting (P14). **(K)** IF staining for H2AK119ub in P14 engrafted skins. Scale=25μm in figures 2C, D, F, G, H, and K. Data in figures (B and E) are presented as boxplots. ***p<0.001; NS, not significant (two-sided t test).
See also Figures S2 and S3.

Figure 3. PRC1 global and catalytic activities are required for Polycomb-mediated transcriptional repression. (A) Differential expression analysis of genes expressed in I53A vs. control (left) and 2KO vs. control (right) in FACS-enriched epidermal progenitor cells. Genes with absolute fold change ≥2 and FDR <0.05 were considered upregulated (red) or downregulated (green). **(B)** Overlap of significantly upregulated genes between I53A and 2KO epidermal cells. **(C)** Percentages of upregulated genes directly occupied by RING1B (left) or H2AK119ub (right). **(D)** RT-qPCR analysis of PRC1 target genes in FACS-enriched epidermal progenitors. n=3. **(E)** Proportion of H3K27me3-bound genes among H2AK119ub(+) upregulated genes. **(F)** SUZ12 ChIP-Seq signal across RING1B-enriched TSS (±5kb) in I53A mutant and control cells **(G)** Whole-mount IF staining for KRT8 in P0 back skins. **(H)** IF staining for Merkel cell markers KRT8 and SOX2 (left). Quantification of KRT8(+) Merkel cells is presented as boxplots (right). n=3. ***p<0.001 (two-sided t test) **(I)** Expression analysis of PRC1 and PRC2 target genes in control, I53A, 2KO, and *Eed* cKO cells. Data are mean ±SEM. **(J)** IGV browser views of RING1B in control and I53A epidermal cells for indicated genes. (**K-L)** ChIP-qPCR for RING1B (K) and H2AK119ub (L) in I53A vs. control epidermal cells. n=3. Data in graphs (D, K, and L) are mean ±SEM. *p<0.05; **p<0.01; ***p<0.001 (two-sided t test).
See also Figure S4 and Table S2.

Figure 4. PRC1 is required for the expression of epidermal and hair follicle developmental genes. (A) Overlap of significantly downregulated genes between I53A and 2KO epidermis. **(B)** GO analysis of downregulated genes in 2KO epidermis. Selected GO terms are in blue. **(C)** RT-qPCR analysis of critical epidermal genes in FACS-enriched 2KO and I53A epidermal cells. n=3. **(D)** IGV browser views of ChIP-seq of RING1B, H2AK119ub, H3K27me3, H3K27ac, H3K4me3, RYBP, and input for indicated genes in control epidermal progenitors. (**E-F)** ChIP-qPCR showing the binding of RING1B (E) and H3K27ac (F) in control epidermal progenitors. Data are mean ±SEM, n=2. **(G)** Overlap of significantly downregulated genes between I53A and 2KO HF cells. **(H)** RT-qPCR analysis of HF lineage genes in 2KO and I53A HFs. n=3. (**I-L)** ChIP-qPCR showing the binding of RING1B and H3K27ac to HF lineage genes in HF-SCs (HF-SC; I-J), outer root sheath cells (ORS; K), and matrix/transient amplifying cells (Mx; L). Data are mean ±SEM, n=2. Data in graphs (C and H) are mean ±SEM. *p<0.05; **p<0.01; ***p<0.001 (two-sided t test).
See also Figure S5 and Tables S2 and S3.

Figure 5. RING1B binding positively regulates gene expression. (A-C) PRC1 loss-of-function analyses in *K14-CreER*; *Ring1a*$^{-/-}$ *Ring1b*$^{flox/flox}$ epidermal progenitor culture upon 4-OHT treatment. (A) Western blot showing changes in RING1B and H2AK119ub protein levels over time. (B) ChIP-qPCR showing changes in RING1B binding. Data are mean ±SEM, n=3. (C) RT-qPCR analysis of changes in the expression of RING1B target genes. Data are mean ±SEM, n=3. (**D-F)** Ring1b overexpression analyses in wild type epidermal progenitor culture. (D) RT-qPCR analysis of endogenous and total Ring1b mRNA. Data are mean ±SEM, n=5. (E) ChIP-qPCR showing changes in RING1B binding. n=3. (F) RT-qPCR analysis of changes in expression of RING1B target genes. n=5. Data in graphs (E and F) are mean ±SEM. *p<0.05; **p<0.01; ***p<0.001 (two-sided t test).
See also Figure S6.

Figure 6. PRC1 complexes function redundantly in skin epithelium development. (A) Heatmap of ChIP-Seq signals across RING1B-peaks for RING1B, H2AK119ub, H3K27me3, H3K27ac, BMI1, CBX8, RYBP, KDM2B, and L3MBTL2 in control epidermal progenitors, with input signal subtracted. **(B)** IGV browser views of RING1B, H3K27me3, H3K27ac, BMI1, CBX8, RYBP, KDM2B, L3MBTL2, and input for indicated genes. (**C-F)** ChIP-qPCR showing the binding of RING1B and RYBP (C), PCGF1 and KDM2B (D),BMI1 and CBX8 (E), and PCGF6 and L3MBTL2 (F) in control epidermal progenitors. Data are mean ±SEM, n=2. Genes with absolute fold change ≥1.8 and false discovery rate (FDR) <0.05 in 2KO vs. control epidermal progenitor cells were

defined as differentially expressed. (**G-I)** H&E analysis of P0 skins of *Pcgf1* cKO, *Pcgf2/4* cKO, *Pcf3/5* cKO, and *Pcgf6* cKO mice compared to controls. Note comparable epidermal thickness (G and H) and HF length (G and I). Quantifications presented in (H and I). n=3. **(J)** IF staining for HF-SC marker SOX9. Scale=25μm. **(K)** IF analysis of KRT8+ Merkel cell numbers. Note the increase in Merkel cells in *Pcgf2/4* cKO skin compared to control. n=4. Scale=100μm in figures 6G and K. Data in figures (H, I and K) are presented as boxplots. ***p<0.001; NS, not significant (two-sided t test).
See also Figure S7 and Table S4.

STAR METHODS

CONTACT FOR REAGENT AND RESOURCE SHARING

Further information and requests for resources and reagents should be directed to and be fulfilled by the Lead Contact, Dr. Elena Ezhkova (elena.ezhkova@mssm.edu).

EXPERIMENTAL MODEL AND SUBJECT DETAILS

Mice

All mice were housed at the Center of Comparative Medicine and Surgery (CCMS), Icahn School of Medicine at Mount Sinai (ISMMS), in accordance with the Institutional Animal Care and Use Committee (IACUC) guidelines (Protocol number LA11-0020). *Krt14-Cre* and *Krt14-CreERT* mice were obtained from the Jackson Laboratories. Immunocompromised *Nude* (NU-Foxn1^{Nu}) mice were obtained from Charles River. *Ring1a*$^{-/-}$, *Ring1b*$^{flox/flox}$, and *Ring1b*^{I53A} were previously described (Cales et al., 2008; del Mar Lorente et al., 2000; Illingworth et al., 2015). Tissue-specific *Krt14-Cre*; *Ring1a*$^{-/-}$ *Ring1b*$^{flox/flox}$ and *Krt14-Cre*; *Ring1a*$^{-/-}$ *Ring1b*$^{I53A/flox}$ mice die shortly after birth, and all analyses of these mice after P0 were done using skin grafting onto *Nude* mice, as previously described (Ezhkova et al., 2011). *Eed*$^{flox/flox}$ and *Suz12*$^{flox/flox}$ mice were generously provided by Weipeng Mu and Terry Magnuson (Mu et al., 2014). *Krt14-RFP* and *Sox9-GFP* reporter mice were previously described (Gong et al., 2003; Zhang et al., 2011). *Krt10-H2B-GFP* transgenic mice were generated by the Mount Sinai Mouse Genetics Shared Resource Facility from an ES cell line, in which the fluorescent GFP reporter is expressed under the control of an 8 kb fragment upstream of TSS of the human *K10* promoter. *Ink4a/Arf*$^{-/-}$ mice were generously provided by Philippe Soriano (Serrano et al., 1996). *Pcgf1*$^{flox/flox}$, *Pcgf3*$^{flox/flox}$, *Pcgf5*$^{flox/flox}$, and *Pcgf6*$^{flox/flox}$ mice were previously described (Almeida et al., 2017; Endoh et al., 2017). *Bmi1(Pcgf2)*$^{flox/flox}$ and *Pcgf4*$^{flox/flox}$ mice were generated in Haruhiko Koseki's lab and will be discussed in a separate manuscript (M.N. and H.K., unpublished). Mice were genotyped by PCR using tail DNA that was extracted using DirectPCR Lysis Reagent, according to manufacturer's instructions (Viagen Biotech Inc., Los Angeles, CA, USA). Primer sequences used for genotyping are available in Table S5. BrdU was administered (50μg per 1g of mouse weight) 4-5 hours before sacrifice.

Cell culture

Primary epidermal progenitors were derived from newborn *K14-CreERT*; *Ring1a*$^{-/-}$ *Ring1b*$^{flox/flox}$ and control mice and maintained in E media, supplemented with 15% serum and 0.3mM CaCl2, on mitomycin C treated

3T3 fibroblasts. After 21 days, epidermal progenitors were trypsinized and grown in E media supplemented with 15% serum and 0.05mM CaCl2. To conditionally delete *Ring1b* in *K14-CreERT*; *Ring1a*$^{-/-}$ *Ring1b*$^{flox/flox}$ culture experiments, cells were treated with 1μM 4-Hydroxytamoxifen (Sigma-Aldrich).

METHOD DETAILS

No randomization or blinding was performed in this study. Sample size is indicated in figure legends and statistical methods are indicated in the quantification and statistical analysis paragraph.

Skin engraftment experiments

Full thickness grafts were performed as previously described (Nowak et al., 2008). Briefly, P0 back skins from sex-matched mice were removed and placed onto the backs of anesthetized female *Nude* recipient mice. In all cases, paired control and I53A or 2KO skins were grafted onto a single *Nude* mouse. Grafts were secured by sterile bandages, which were removed 12-13 days after grafting. Split-thickness grafts were performed as previously described (Nowak et al., 2008). For split-thickness grafts, back skins of P0 mice were placed with the dermis facing down in 5mM EDTA in 1x PBS for 1 hour at 37ºC. Prior to grafting, the epidermis was removed from the HF/dermis, which was then grafted using the same procedure as that used for full thickness grafts.

Construction of Ring1b expression vectors

The full length Ring1b coding sequence was PCR-amplified and cloned into a pGEM-T Easy vector (Promega; Madison,WI, USA). Point mutation of I53A in Ring1b was introduced into the wild type Ring1b construct using Phusion High-Fidelity DNA polymerase (New England Biolabs) by PCR amplification, followed by DpnI enzymatic digestion (New England Biolabs). These were then sub-cloned into the mammalian expression vector pHAGE-IRES-ZsGreen to generate pHAGE-Ring1b and pHAGE-Ring1b^{I53A} expression vectors. Both constructs were sequenced to confirm their sequence and orientation. Primer sequences used for cloning are available in Table S5.

Ring1b overexpression in primary epidermal progenitor culture

For lentivirus production, HEK293T cells were transfected by calcium phosphate transfection with pHAGE-IRES-ZsGreen plasmids, and helper plasmids psPAX2 and PMD2.G. psPAX2 and PMD2.G plasmids were a gift from Didier Trono (Addgene plasmids #12260 and #12259). Viral supernatant was collected 48 hours post-transfection, and filtered through 0.45 μm filter. Lentiviral particles were concentrated by ultracentrifugation for 2.5 hours at 25,000 rpm and the pellet was resuspended in cold E media. Control epidermal progenitors cells were then transduced with viral stock that expressed the pHAGE-Ring1b^{I53A}, pHAGE-Ring1b, or a control pHAGE-IRES-ZsGreen empty vector, and supplemented with 4μg/ml polybrene (Sigma-Aldrich). Virus-

containing media was replaced after 8 hours by fresh E media. GFP^{low} cells were selected by flow cytometry, expanded in culture, and then collected for ChIP-qPCR and RT-qPCR analyses.

Fluorescence-activated cell sorting

Basal layer epidermal progenitors were isolated from *Krt14-RFP* and *Krt10-H2B-GFP* newborn mice. Briefly, P0 back skins were collected and incubated for 4-6 hours in 1.26U/mL dispase (Invitrogen) at 4ºC. The epidermis was gently peeled from the underlying dermis, dissociated by 0.25% Trypsin with 2.21mM EDTA (Corning Cellgro; Manassas, VA, USA) and washed twice with 1x PBS. Cells were stained with 1:200 Sca1-APC ((Biolegend; San Diego, CA, USA) for 30 minutes on ice and washed twice with 1x HBSS prior to cell sorting. Epidermal progenitors were sorted as SCA1(+),RFP(high), and GFP(-); differentiated epidermal suprabasal cells (SB) were collected as a control and sorted as SCA1(+),RFP(high), and GFP(+). For RNA and RNA-Seq analysis of control, *Krt14-Cre Ring1a*$^{-/-}$ *Ring1b*$^{I53A/flox}$, and *Krt14-Cre Ring1a*$^{-/-}$ *Ring1b*$^{flox/flox}$ mice, newborn P0 back skins were collected and subjected to 0.25% collagenase digestion for 60 minutes at 37ºC with 80 rpm shaking, followed by 0.25% trypsin treatment for 15 minutes at 37ºC. The cell suspension was washed twice with 1x PBS, stained with 1:200 SCA1-PerCP-Cy5.5 (Biolegend), 1:100 α6-integrin-FITC (eBiosciences), and 1:200 EPCAM-APC (Biolegend) for 30 minutes on ice, and washed twice with 1x HBSS prior to cell sorting. Interfollicular epidermis, enriched for epidermal progenitors, was sorted as EPCAM(+), SCA1(+), and α6-integrin(high); hair follicle cells were sorted as EPCAM(+), Sca1(-), and α6-integrin(+). For ChIP and ChIP-Seq analyses of control and *Krt14-Cre Ring1a*$^{-/-}$ *Ring1b*$^{I53A/flox}$ mice, P0 back skins were collected and incubated for 4-6 hours in 1.26U/ml dispase at 4ºC. The epidermis was gently peeled from the underlying dermis, dissociated by 0.25% trypsin, and washed twice with 1x PBS. Cells were stained with 1:200 SCA1-PerCP-Cy5.5 (Biolegend), 1:100 α6-integrin-FITC (eBiosciences), and 1:200 EPCAM-APC (Biolegend) for 30 minutes on ice, and washed twice with 1x HBSS prior to cell sorting. Epidermal progenitor cells were sorted as EPCAM(+), Sca1(+), and α6-integrin(high). For hair follicle ChIP analysis, *Krt14-RFP* and *Sox9-GFP* P4.5 back skins were collected and incubated for 4-6 hours in 1.26U/mL dispase at 4ºC. The epidermis was gently peeled from the underlying dermis and the remaining dermis was dissociated with collagenase for 1 hour at 37ºC and washed twice with 1x PBS, followed by low speed centrifugation at 20g for 5 minutes to enrich pellets for hair follicle cells. Pellets were then incubated with trypsin at 37ºC for 15 minutes to generate single cell suspensions of hair follicle cells, as previously described (Wang et al., 2013). Cells were stained with 1:200 SCA1-APC and 1:100 α6-integrin-APC-Cy7. Hair follicle Mx was sorted as SCA1(-), RFP(low), GFP(-), and α6-integrin(+); hair follicle ORS was sorted as Sca1(-), RFP(high), GFP(-), and α6-integrin(high); HF-SCs were sorted as SCA1(-), RFP(high), GFP(+), and α6-integrin(high). All cell isolations were performed on a FACS Influx instrument (BD, Franklin Lakes, NJ, USA) in the Flow Cytometry Core Facility at Icahn School of Medicine at Mount Sinai.

Chromatin immunoprecipitation, ChIP-qPCR and library preparation

Chromatin immunoprecipitation (ChIP) was performed on FACS-sorted populations using materials and methods as previously described (Lien et al., 2011). A total of 0.4 x 10^6 cells was used for each histone mark per ChIP, and a total of 6 x 10^6 cells was used for each Polycomb subunit per ChIP. Prior to cell sorting, cells were stained for viability using Zombie violet (Biolegend; San Diego, CA), then cross-linked using fresh solution with a final concentration of 1% formaldehyde (Thermo Fisher Scientific; Rockford, IL) for 10 minutes at room temperature. Crosslinking was stopped by the addition of Glycine (final concentration 125mM) for 5 minutes of incubation at room temperature, followed by two washes with 1x PBS. Cells were incubated in lysis buffer 1 (50mM HEPES pH=7.5, 140mM Nacl, 1mM EDTA, 10% glycerol, 0.5% NP-40, 0.25% Triton X-100, protease inhibitor cocktail (Roche)) for 10 min on ice, then incubated for 10 min with lysis buffer 2 (10mM Tris-HCl pH=7.5, 200mM NaCl, 1mM EDTA, 0.5mM EGTA). Before ChIP, cells were resuspended in lysis buffer 3 (10mM Tris-HCl pH=8.0, 200mM NaCl, 1mM EDTA, 0.5mM EGTA, 0.1% Na-deoxycholate, 0.5% N-laurylsarcosine, 1% Triton X-100) and sonicated using a Bioruptor Sonicator (Diagenode, UCD-200) according to a 25x regimen of 30 seconds of sonication followed by 90 seconds of rest at 2.7ºC. Chromatin was incubated overnight at 4ºC with antibodies as indicated in Table S5. Dynal protein G magnetic beads (Invitrogen) were added the next day and incubated for 4 hours. The beads were sequentially washed with low salt, high salt, LiCl, and Tris-EDTA buffers for 10 minutes each at 4ºC. Bound chromatin was eluted and crosslinking was reversed by overnight incubation at 65ºC, followed by RNase A (Sigma-Aldrich) and proteinase K (Roche Diagnostics) treatments. Samples were purified using ChIP DNA Clean and Concentrator kit (Zymo Research; Irvine, CA). Samples were analyzed by qPCR using LightCycler® 480 SYBR Green I Master Mix (Roche Diagnostics) on a Lightcycler 480 instrument (Roche). Primer sequences are available in Table S5. For high-throughput ChIP sequencing, libraries were constructed from 3ng of Purified DNA using the DNA SMART ChIP-Seq Kit (Clontech; Palo Alto, CA, USA) according to the manufacturer's instructions. Constructed ChIP-seq libraries were sequenced on the Illumina HiSeq 4000 platform, and two biological replicates were used.

RNA purification, RT-qPCR, and library preparation

FACS-purified cells were collected directly into RLT Plus buffer (QIAGEN), and total RNA was isolated with the RNeasy Plus Micro Kit (QIAGEN). Complimentary DNA was reverse-transcribed from total RNA using qScript cDNA SuperMix (Quanta Biosciences, Gaithersburg, MD, USA) according to the manufacturer's instructions. Samples were analyzed by RT-qPCR using LightCycler® 480 SYBR Green I Master Mix (Roche Diagnostics) on a Lightcycler 480 instrument (Roche). Results were normalized to Ppib mRNA levels. Primer sequences are available in Table S5. Prior to library construction, sample quality was measured using an Agilent Bioanalyzer, and samples with RNA integrity numbers > 8 were used. 10ng of RNA were reverse transcribed and amplified using the Ovation RNA-seq System V2 (Nugen). Libraries were constructed from 100ng of sonicated cDNA (Covaris) using the Ovation Ultra Low DR Multiplex system (Nugen). The concentration and quality of the libraries were determined using Qubit (Invitrogen) and Bioanalyzer (Agilent). Constructed RNA-seq libraries were sequenced on the Illumina HiSeq 2500 platform, obtaining 100-nucleotide single reads.

Western Blotting

P0 back skins were collected and incubated for 4-6 hours in 1.26U/ml dispase (Invitrogen) at 4ºC. The epidermis was gently peeled from the underlying dermis, dissociated by 0.25% Trypsin (Corning Cellgro), and washed twice with 1x PBS. Total cell lysate was prepared by addition of EZ lysis buffer (60mM Tris-HCl pH=6.8, 10% glycerol, 2% SDS) for 10 minutes at 95ºC. Samples (50 µg) were run on 12% SDS-PAGE, transferred to PVDF membranes, and analyzed with the indicated antibodies (Table S5).

Immunohistochemistry

Formalin fixed paraffin-embedded 5µm sections of normal human skin were obtained from IHC World Tissue Bank (IHC world, Woodstock, MD, USA). Sections were deparaffinized in xylene, rehydrated in decreasing concentrations of ethanol, and treated with 3% H_2O_2 in methanol for 10 min. Tissues were then subjected to antigen retrieval with 10mM citrate buffer pH=6.0, and stained with rabbit anti-RING1B antibodies (1:250), rabbit anti-H2AK119ub antibodies (1:500), or control rabbit IgG antibodies for 1 hour at room temperature. The slides were then incubated with secondary anti-rabbit conjugated to HRP using the VECTRASTAIN ABC kit according to the manufacturer's instructions (Vector Laboratories, Burlingame, CA, USA), and the staining was developed using the DAB peroxidase substrate kit (Vector Laboratories). To identify nuclei, slides were briefly counterstained with hematoxylin.

Immunofluorescence staining and microscopy

Back skin tissues were collected from mice, embedded in OCT compound (Tissue-Tek, Torrance, CA, USA), and subsequently cut into 7µm sections using a Leica Cryostat. Slides were then pre-fixed in 4% PFA for 10min at room temperature and blocked overnight at 4ºC in blocking solution (1x PBS supplemented with 0.1% Triton X-100, 1% BSA, 0.25% normal donkey serum, 0.01% gelatin). Primary antibodies were diluted in blocking solution and incubated for 1 hour, followed by 1-hour incubation with secondary antibodies. Slides were counterstained with DAPI to visualize nuclei. Whole-mount immunofluorescence was performed as previously described (Perdigoto et al., 2016). Briefly, back skins were collected from newborn mice and placed in 1.26U/mL dispase for 4 hours at 4ºC. The epidermis was gently peeled from the underlying dermis and fixed in 4% PFA for 1 hour at 4ºC. Skins were blocked for 2 hours at room temperature and incubated with primary antibodies overnight at 4ºC, followed by incubation with secondary antibodies for 2 hours at room temperature. TUNEL apoptosis detection assay was performed using the In Situ Cell Death Detection Kit, Fluorescein (Roche). All antibodies and dilutions are available in Table S5. Slides were imaged using a Leica DM5500 slide microscope using 5x, 10x, or 20x objectives.

QUANTIFICATION AND STATISTICAL ANALYSIS

ChIP-Seq analysis and data visualization

ChIP-seq reads were trimmed by 3 bases at the 5' end using Trim Galore (v0.4.1; http://www.bioinformatics.babraham.ac.uk/projects/trim_galore/) prior to alignment, as recommended by the ChIP kit manufacturer. The trimmed reads were then aligned to the mm10 reference genome using either bowtie (v1.1.1, for samples of 50bp read length; http://bowtie-bio.sourceforge.net/index.shtml) or bowtie2 (v2.2.3, for samples of 100bp read length; http://bowtie-bio.sourceforge.net/bowtie2/index.shtml). Only uniquely aligned reads were kept for downstream analysis, with duplicate reads removed by the Samtools software v0.1.19 (Li et al., 2009). The aligned reads were also filtered for ChIP kit specific artifacts (https://github.com/dzhaobio/SMARTcleaner). Peaks from RYBP, BMI1, CBX8, KDM2B, L3MBTL2, and AUTS2 ChIP-seq were called using the MACS2 software (v2.1.0; https://github.com/taoliu/MACS) with inputs serving as controls, and default settings. Peaks (mostly broad) in H3K27me3, H2AK119ub1, and RING1B were called as previously described (Goldberg et al., 2010). Peaks called from the two biological replicates were merged to generate a union list of peaks, because nearly all peaks called from one replicate also exhibit strong signals in the other replicates (as shown in Fig 1B and 6A), indicating the "replicate-specific" peaks were a result of thresholding by software. For example, the RING1B peaks from the two replicates show >80% overlap and a Pearson's correlation coefficient of 0.99 (based on ChIP-seq read densities in the union peaks). As such, we took the union of the peaks called from the two replicates as our final peaks. Peaks were classified as promoter (within 2kb of transcription start sites), gene body (within a gene), distal (<50kb from genes), or intergenic peaks, based on their chromosomal distances to a reference gene. To cluster Ring1b peaks, we randomly sampled 5 million reads from each of the ChIP-seq samples and used them as inputs to the seqMINER v1.3.4 (Ye et al., 2011) for K-means clustering analysis. The read density matrix (+/- 5kb from the RING1B peak centers) from the seqMINER was imported to the R package pheatmap for drawing heatmaps, with signal of input subtracted. When we counted the numbers of genes in each cluster, we associated a gene to the cluster to which its largest peak was mapped, for a gene with multiple peaks. To visualize ChIP-seq signal at individual genomic regions, we used the Integrative Genomics Viewer (IGV; http://software.broadinstitute.org/software/igv/) and TDF files from the igvtools (v2.3.57; https://software.broadinstitute.org/software/igv/igvtools).

RNA-Seq analysis and data visualization

RNA-seq reads were aligned to the mouse reference genome (mm10) using Tophat (v2.0.13; https://ccb.jhu.edu/software/tophat/index.shtml) gene models of Refgene were downloaded from the UCSC genome browser on March 13, 2017. FPKM (Fragments Per Kilobase of transcript per Million mapped reads) values were generated using cufflinks (v2.2.1; http://cole-trapnell-lab.github.io/cufflinks/). Lowly expressed genes (mean FPKM values < 1 in both groups under comparison) were excluded from differential expression analysis. We analyzed read counts from the HTSeq (v0.6.1; https://github.com/simon-anders/htseq) for differential analysis, using the DESeq2 v1.6.3 (Love et al., 2014), and considered genes with fold change >2 and false discovery rate (FDR) < 0.05 as significantly differentially expressed. To visualize RNA-seq signal at

individual genomic regions, we used the Integrative Genomics Viewer (IGV) and TDF files from igvtools (v2.3.57).

Gene Ontology enrichment analysis

Identification of significantly over-represented functional categories was done using DAVID (Huang da et al., 2009). For RING1B-clusters, the entire gene list for each cluster was functionally annotated for biological processes. Selected GO terms were considered significant with $p<0.05$ and are shown in Figure 1F and Table S1. Genes significantly downregulated in 2KO vs. control epidermal progenitors were annotated using same significance parameters and selected GO terms are shown in Figure 4B and Table S2. Genes significantly downregulated in 2KO vs. control hair follicle cells were annotated using same significance parameters and selected GO terms are shown in Figure S5G and Table S3.

Quantification of epidermal thickness and hair follicle length

Epidermal thickness measurements were made from the bottom of the basal layer to the top of the stratum corneum using the Leica LAS AF software. Measurements of hair follicle length were made from the bottom of the hair follicle to the start of epidermis basal layer using the Leica LAS AF software. At least 200 random epidermal regions and hair follicles were measured for each animal group, from three animals (n=3) of two independent litters. Comparisons and statistics were performed between matching knockout and control littermates.

Cell proliferation analysis and quantification of BrdU(+) cells

BrdU(+) cells in the basal layer of the epidermis where quantified using the Leica LAS AF software. Nuclear DAPI staining was used to quantify the total number of cells in the basal layer, and the data are shown as the percentage of BrdU(+) cells in the basal layer. For quantification of BrdU(+) cells in the hair follicles, skins were counterstained with KRT5, and BrdU(+) cells were quantified in KRT5(+) hair follicle cells. Nuclear DAPI staining was used to quantify the total number of cells in the KRT5(+) hair follicles, and data are shown the percentage of BrdU(+) cells in hair follicles. At least 50 random epidermal regions and hair follicles were measured for each animal group, from three animals (n=3) of two independent litters. Comparisons and statistics were performed between matching knockout and control littermates.

Quantification of KRT8(+) Merkel cells

Merkel cells were quantified by the number of KRT8(+) cells per millimeter (mm) of skin. Sections had typical skin length ranging between 7-14 mm. At least 100 mm of total skin length was analyzed per condition, from at least three animals ($n\geq3$) of two independent litters. Comparisons and statistics were performed between matching knockout and control littermates.

Statistics

To determine the statistical significance of overlap between ChIP-seq and RNA-seq data, a Fisher's exact test was performed. To determine the statistical significance between two groups, a two-sided t test was performed. To determine the statistical significance between more than two groups, comparisons were made using one-way ANOVA with the Bonferroni post-hoc test. Box-and-whisker boxplots are minimum-to-maximum: midline, median; box limits, 25^{th} percentile (lower quartile) and 75^{th} percentile (upper quartile); upper whisker, 75^{th}-100^{th} percentile; lower whisker, 0-25^{th} percentile. For boxplots in Figures 1A, S4G, S4H, and 5SB: midline, median; box limits, 25^{th} percentile (lower quartile) and 75^{th} percentile (upper quartile); upper whisker, 75^{th}-95^{th} percentile; lower whisker, 5^{th}-25^{th} percentile. All data in bar graphs are presented as mean ±SEM. The number of biological replicates used for comparison is indicated in each figure. For each comparison, at least 3 animals for each group from two independent litters were used. Significance levels were defined as *p<0.05; **p<0.01; ***p<0.001; NS, not significant. For statistical analyses GraphPad Prism 5 was used.

DATA AND SOFTWARE AVAILABILITY

The accession number for the sequencing data reported in this paper is NCBI GEO: GSE112460

Supplemental Information

Supplemental Tables:

Table S1. PRC1 chromatin binding profiling in epidermal progenitors, related to Figures 1 and S1.

Table S2. Differential expression analysis of genes expressed in I53A vs. control and 2KO vs. control FACS-enriched epidermal progenitor cells, related to Figures 3, 4, S4, and S5.

Table S3. Differential expression analysis of genes expressed in I53A vs. control and 2KO vs. control FACS-purified HF cells, related to Figures 4, S4 and S5.

Table S4. Analysis of RING1B/AUTS2 co-bound genes in epidermal progenitors, related to Figures 6 and S7.

Table S5. List of antibodies, genotyping primers, cloning primers, RT-qPCR primers, and ChIP-qPCR primers used in this study, related to STAR Methods.

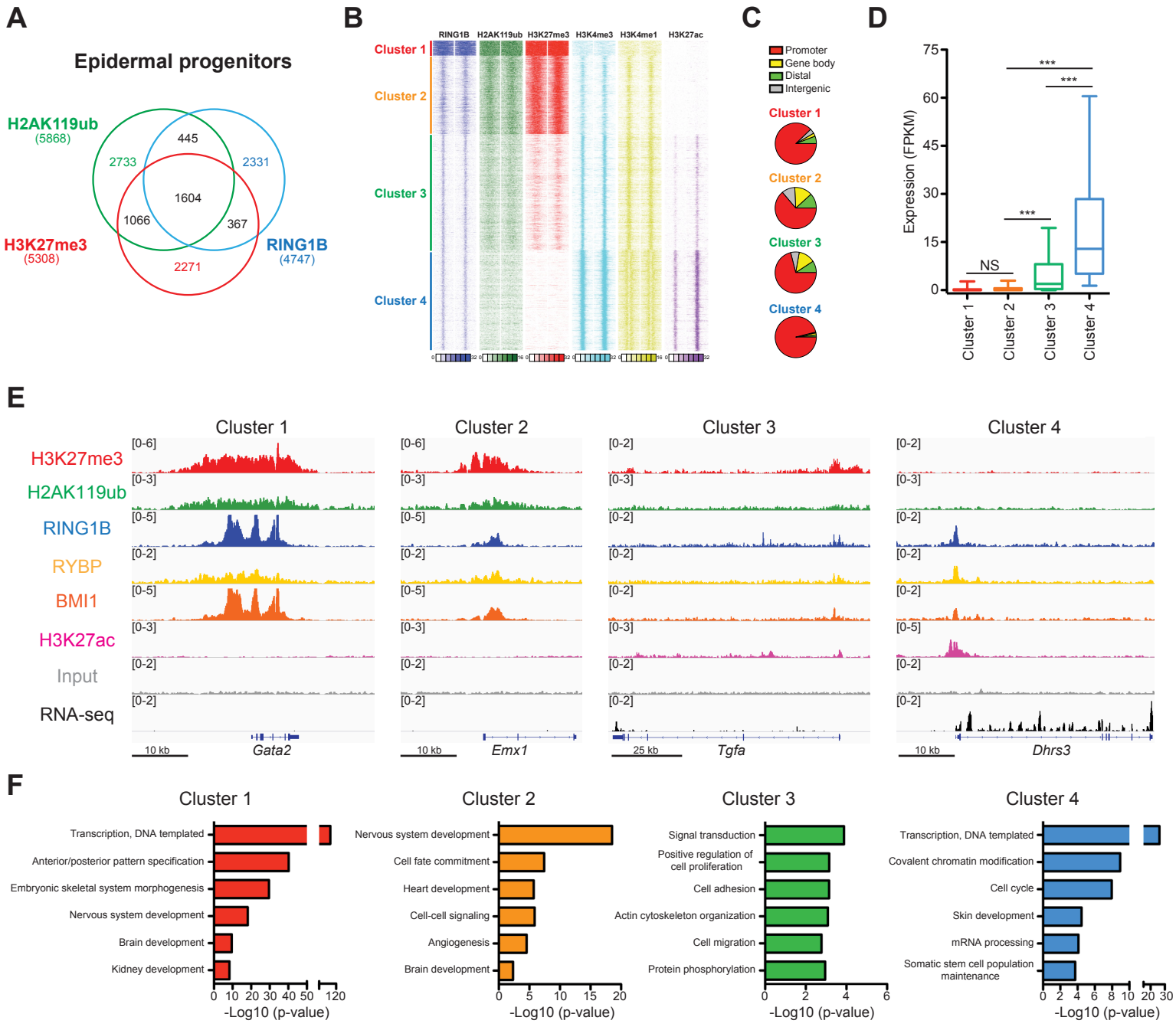
A
Epidermal progenitors
H2AK119ub
(5868)
H3K27me3
(5308)
RING1B
(4747)
445
2733
2331
1604
1066
367
2271
B
RING1B
H2AK119ub
H3K27me3
H3K4me3
H3K4me1
H3K27ac
Cluster 1
Cluster 2
Cluster 3
Cluster 4
C
Promoter
Gene body
Distal
Intergenic
Cluster 1
Cluster 2
Cluster 3
Cluster 4
D
Expression (FPKM)
75
60
45
30
15
0
***
***
***
NS
Cluster 1
Cluster 2
Cluster 3
Cluster 4
E
Cluster 1
Cluster 2
Cluster 3
Cluster 4
H3K27me3
H2AK119ub
RING1B
RYBP
BMI1
H3K27ac
Input
RNA-seq
[0-6]
[0-3]
[0-5]
[0-2]
10 kb
Gata2
Emx1
25 kb
Tgfa
Dhrs3
F
Cluster 1
Transcription, DNA templated
Anterior/posterior pattern specification
Embryonic skeletal system morphogenesis
Nervous system development
Brain development
Kidney development
-Log10 (p-value)
Cluster 2
Nervous system development
Cell fate commitment
Heart development
Cell-cell signaling
Angiogenesis
Brain development
-Log10 (p-value)
Cluster 3
Signal transduction
Positive regulation of cell proliferation
Cell adhesion
Actin cytoskeleton organization
Cell migration
Protein phosphorylation
-Log10 (p-value)
Cluster 4
Transcription, DNA templated
Covalent chromatin modification
Cell cycle
Skin development
mRNA processing
Somatic stem cell population maintenance
-Log10 (p-value)

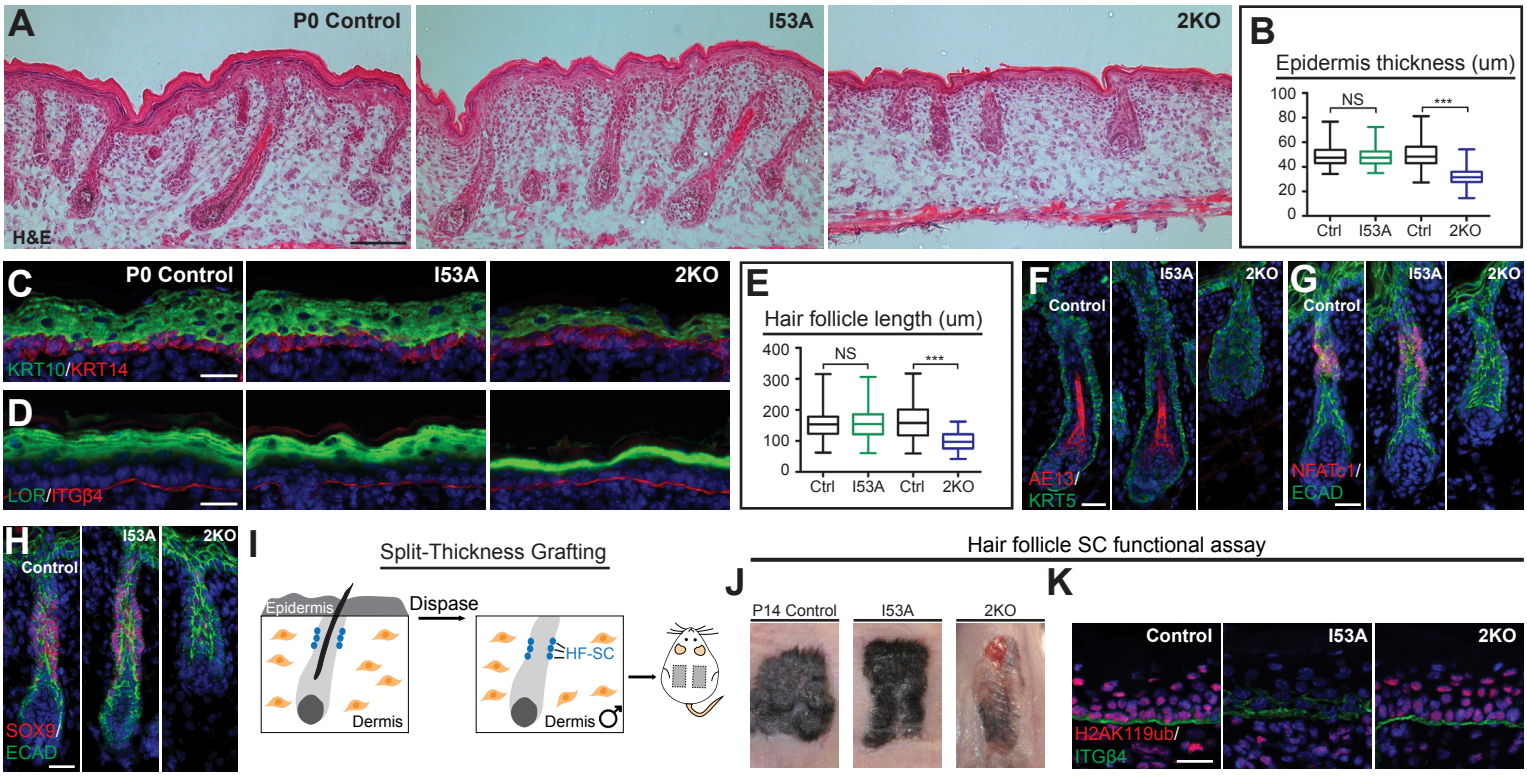
A
P0 Control
I53A
2KO
H&E
B
Epidermis thickness (um)
100
80
60
40
20
0
NS
***
Ctrl
I53A
Ctrl
2KO
C
P0 Control
I53A
2KO
KRT10/KRT14
D
LOR/ITGβ4
E
Hair follicle length (um)
400
300
200
100
0
NS
***
Ctrl
I53A
Ctrl
2KO
F
Control
I53A
2KO
AE13/
KRT5
G
Control
I53A
2KO
NFATc1/
ECAD
H
Control
I53A
2KO
SOX9/
ECAD
I
Split-Thickness Grafting
Epidermis
Dispase
Dermis
HF-SC
Dermis
Hair follicle SC functional assay
J
P14 Control
I53A
2KO
K
Control
I53A
2KO
H2AK119ub/
ITGβ4

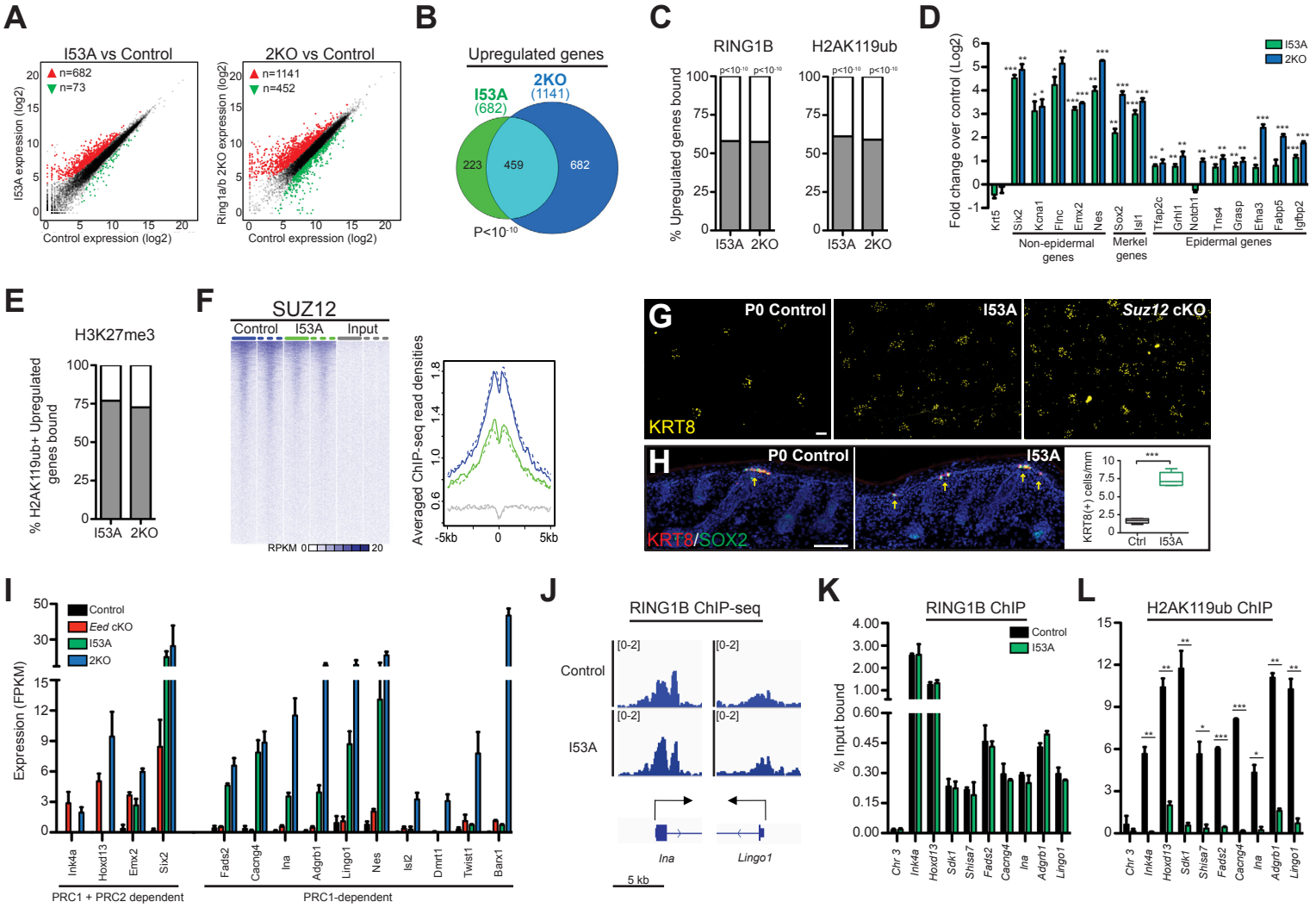
A
I53A vs Control
n=682
n=73
I53A expression (log2)
Control expression (log2)
2KO vs Control
n=1141
n=452
Ring1a/b 2KO expression (log2)
Control expression (log2)
B
Upregulated genes
I53A (682)
2KO (1141)
223
459
682
P<10-10
C
RING1B
H2AK119ub
% Upregulated genes bound
I53A 2KO
D
I53A
2KO
Fold change over control (Log2)
Krt5 Six2 Kcna1 Flnc Emx2 Nes Sox2 Isl1 Tfap2c Grhl1 Notch1 Tns4 Grasp Efna3 Fabp5 Igfbp2
Non-epidermal genes
Merkel genes
Epidermal genes
E
H3K27me3
% H2AK119ub+ Upregulated genes bound
I53A 2KO
F
SUZ12
Control I53A Input
RPKM 0 20
Averaged ChIP-seq read densities
-5kb 0 5kb
G
P0 Control
I53A
Suz12 cKO
KRT8
H
P0 Control
I53A
KRT8/SOX2
KRT8(+) cells/mm
Ctrl I53A
I
Control
Eed cKO
I53A
2KO
Expression (FPKM)
Ink4a Hoxd13 Emx2 Six2 Fads2 Cacng4 Ina Adgrb1 Lingo1 Nes Isl2 Dmrt1 Twist1 Barx1
PRC1 + PRC2 dependent
PRC1-dependent
J
RING1B ChIP-seq
Control
I53A
[0-2]
Ina
Lingo1
5 kb
K
RING1B ChIP
Control
I53A
% Input bound
Chr 3 Ink4a Hoxd13 Sdk1 Shisa7 Fads2 Cacng4 Ina Adgrb1 Lingo1
L
H2AK119ub ChIP
Chr 3 Ink4a Hoxd13 Sdk1 Shisa7 Fads2 Cacng4 Ina Adgrb1 Lingo1

Skin Epidermis Analysis

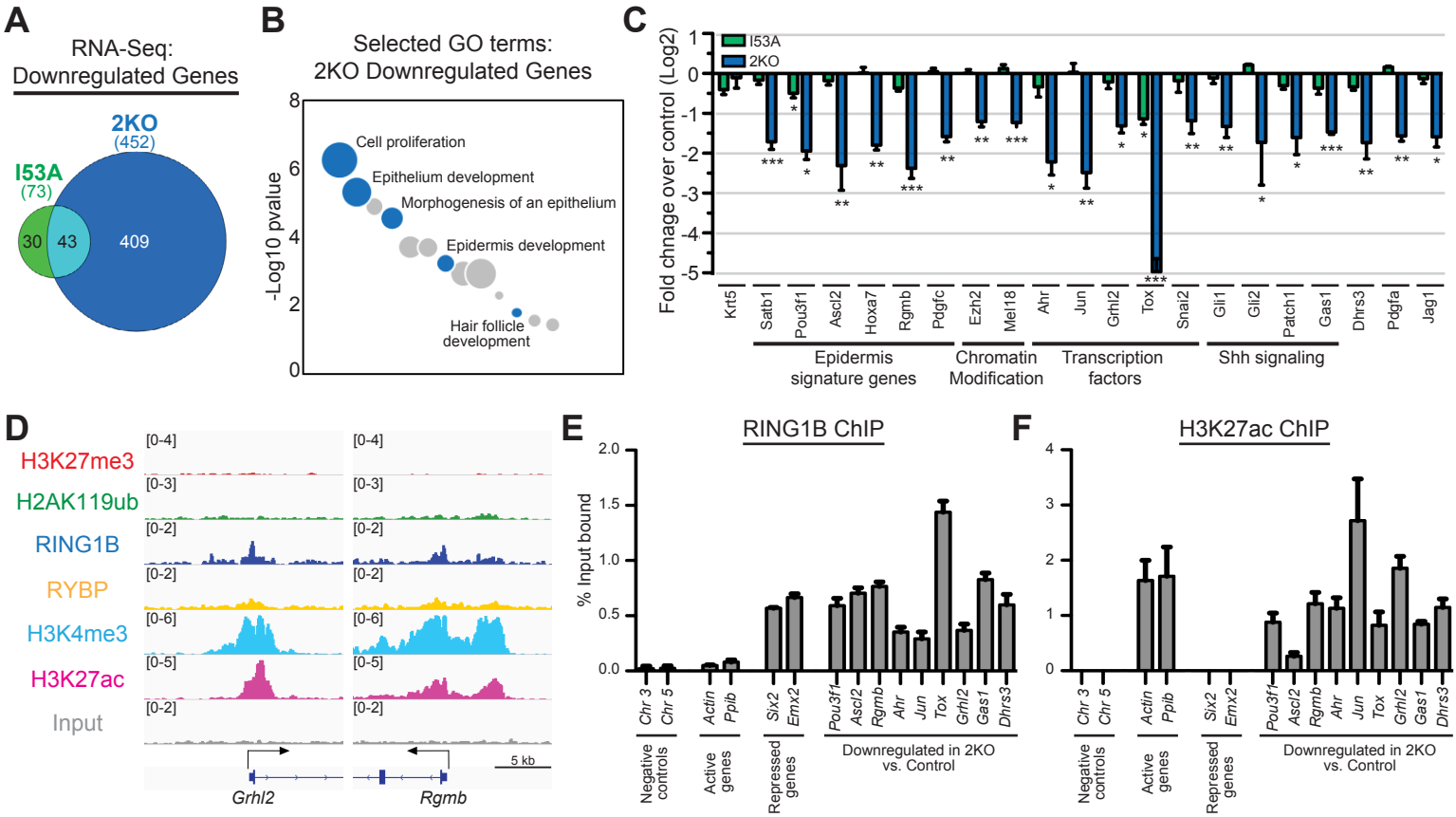

Hair follicle Analysis

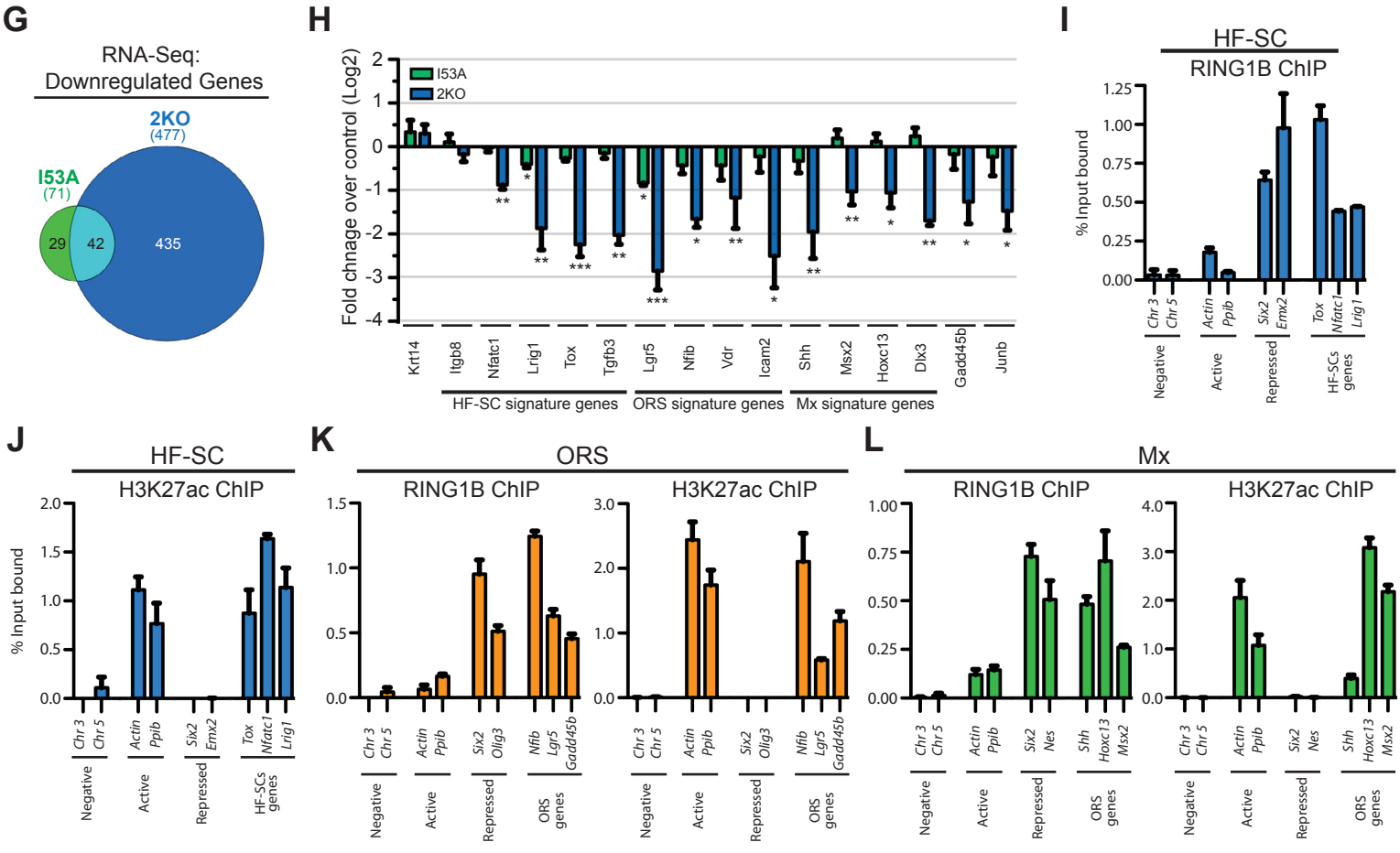

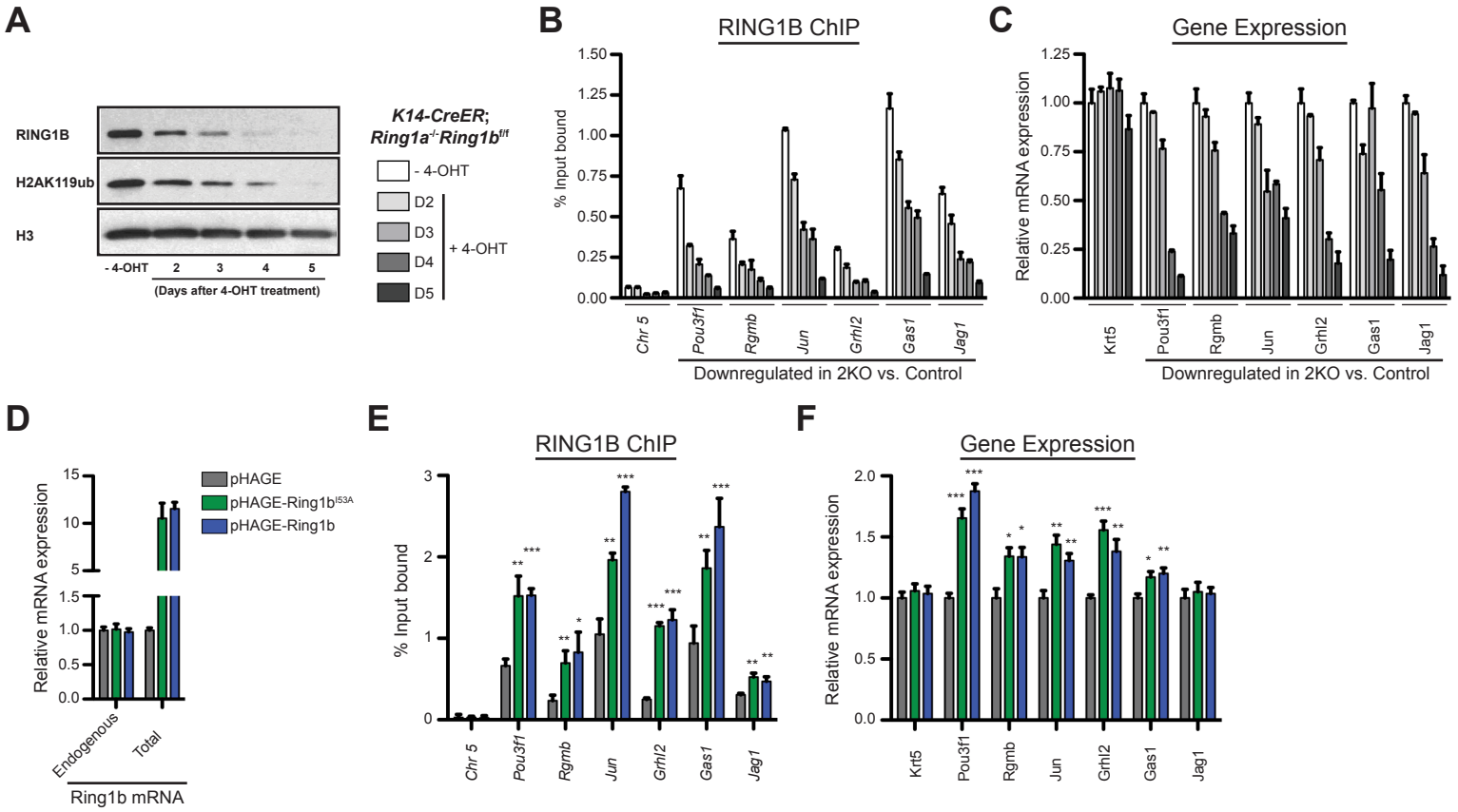
A
RING1B
H2AK119ub
H3
- 4-OHT
2
3
4
5
(Days after 4-OHT treatment)
K14-CreER;
Ring1a-/-Ring1bf/f
- 4-OHT
D2
D3
D4
D5
+ 4-OHT
B
RING1B ChIP
% Input bound
1.50
1.25
1.00
0.75
0.50
0.25
0.00
Chr 5
Pou3f1
Rgmb
Jun
Grhl2
Gas1
Jag1
Downregulated in 2KO vs. Control
C
Gene Expression
Relative mRNA expression
1.25
1.00
0.75
0.50
0.25
0.00
Krt5
Pou3f1
Rgmb
Jun
Grhl2
Gas1
Jag1
Downregulated in 2KO vs. Control
D
Relative mRNA expression
15
10
5
1.5
1.0
0.5
0.0
pHAGE
pHAGE-Ring1bI53A
pHAGE-Ring1b
Endogenous
Total
Ring1b mRNA
E
RING1B ChIP
% Input bound
3
2
1
0
Chr 5
Pou3f1
Rgmb
Jun
Grhl2
Gas1
Jag1
F
Gene Expression
Relative mRNA expression
2.0
1.5
1.0
0.5
0.0
Krt5
Pou3f1
Rgmb
Jun
Grhl2
Gas1
Jag1

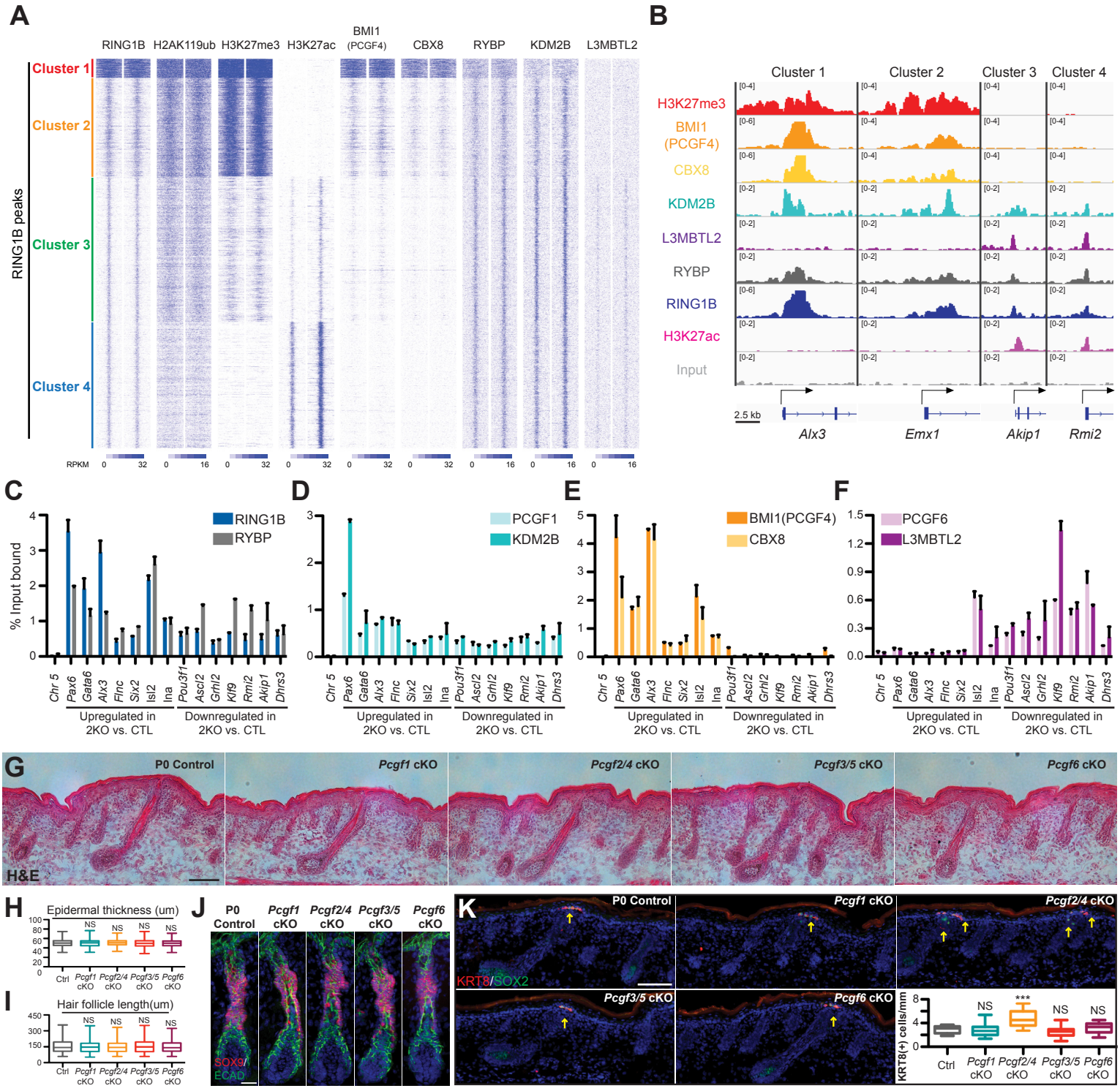
A
RING1B
H2AK119ub
H3K27me3
H3K27ac
BMI1 (PCGF4)
CBX8
RYBP
KDM2B
L3MBTL2
Cluster 1
Cluster 2
Cluster 3
Cluster 4
RING1B peaks
RPKM
B
Cluster 1
Cluster 2
Cluster 3
Cluster 4
H3K27me3
BMI1 (PCGF4)
CBX8
KDM2B
L3MBTL2
RYBP
RING1B
H3K27ac
Input
2.5 kb
Alx3
Emx1
Akip1
Rmi2
C
% Input bound
RING1B
RYBP
Upregulated in 2KO vs. CTL
Downregulated in 2KO vs. CTL
D
PCGF1
KDM2B
E
BMI1(PCGF4)
CBX8
F
PCGF6
L3MBTL2
Chr 5
Pax6
Gata6
Alx3
Flnc
Six2
Isl2
Ina
Pou3f1
Ascl2
Grhl2
Klf9
Rmi2
Akip1
Dhrs3
G
P0 Control
Pcgf1 cKO
Pcgf2/4 cKO
Pcgf3/5 cKO
Pcgf6 cKO
H&E
H
Epidermal thickness (um)
NS
Ctrl
I
Hair follicle length(um)
J
SOX9/ECAD
K
KRT8/SOX2
KRT8(+) cells/mm
***